Nuclear Singlet Relaxation by Scalar Relaxation of the Second Kind in the Slow-Fluctuation Regime

S.J. Elliott,[1, a)] C. Bengs,[1] L.J. Brown,[1] J.T. Hill-Cousins,[1, b)] D.J. O'Leary,[2] G. Pileio,[1] and M.H. Levitt[1, c)]
[1)] *School of Chemistry, University of Southampton, Southampton SO17 1BJ, United Kingdom*
[2)] *Department of Chemistry, Pomona College, Claremont, CA 91711, United States of America*

(Dated: 24 January 2019)

The singlet state of nuclear spin-1/2 pairs is protected against many common relaxation mechanisms. Singlet order, which is defined as the population difference between the nuclear singlet and triplet states, usually decays more slowly than the nuclear magnetization. Nevertheless, some decay mechanisms for nuclear singlet order persist. One such mechanism is called scalar relaxation of the second kind (SR2K), and involves the relaxation of additional nuclei ("third spins") which have scalar couplings to the spin-1/2 pair. This mechanism requires a difference between the couplings of at least one third spin with the two members of the spin-1/2 pair, and depends on the longitudinal relaxation time of the third spin. The SR2K mechanism of nuclear singlet relaxation has previously been examined in the case where the relaxation rate of the additional spins is on the timescale of the nuclear Larmor frequency. In this paper we consider a different regime, in which the longitudinal relaxation of the third spins is on a similar timescale to the J-coupling between the members of the spin pair. This regime is often encountered when the spin-1/2 pair has scalar couplings to nearby deuterium nuclei. We show that the SR2K mechanism may be suppressed in this regime by applying a radiofrequency field which is resonant either with the members of the spin pair, or with the third spins. These phenomena are analyzed theoretically and by numerical simulations, and demonstrated experimentally on a diester of $[^{13}C_2,^2H_2]$-labelled fumarate in solution.

I. INTRODUCTION

Clusters of spin-1/2 nuclei may form magnetically "silent" configurations which are sheltered from NMR relaxation and decay with extended lifetimes[1–46]. These long-lived states (LLS) may have decay rate constants which greatly exceed that of longitudinal magnetization. A long-lived state lifetime has surpassed the relaxation time constant T_1 by a factor of 50 in one case[27,28], and a lifetime exceeding 1 hour was observed for a naphthalene derivative in solution[33]. Experiments have been performed in which LLS phenomena are combined with hyperpolarization methodology in order to generate nuclear spin systems which are far from equilibrium, and to maintain the non-equilibrium state for extended time intervals[8,19,20,43,47]. There are potential applications to molecular imaging[27,28].

In the case of spin-1/2 pairs, the LLS is called *singlet order* and is defined as the population imbalance between the spin-0 singlet state and the spin-1 triplet states[1,2]. The nuclear singlet state is antisymmetric with respect to particle exchange, while the three nuclear triplet states are exchange-symmetric. Small differences in chemical shift between the participating spins, or differential scalar couplings to spins outside the pair, allow experimental access to the nuclear singlet order using suitable radiofrequency pulse sequences[10,13,18,22]. The decay time constant of singlet order is denoted T_S.

In solution, the dominant relaxation mechanism for the nuclear magnetization of spin-1/2 pairs is often the stochastic modulation of the dipole-dipole coupling between the two nuclei by the molecular tumbling (the "in pair DD mechanism"). This can be a strong mechanism for the decay of nuclear magnetization, but does not lead to a decay of nuclear singlet order. As a result, T_S may exceed T_1 by a large factor.

Several mechanisms contribute to the rate constant ${T_S}^{-1}$ for the decay of singlet order. These include: motional modulation of dipole-dipole couplings to nuclear or electronic spins outside the pair, either in the same molecule or other molecules[11,12,16,36]; chemical shift anisotropy, involving both the symmetric and the antisymmetric parts of the chemical shift tensors[16,33,34]; spin-rotation interactions, involving the coupling of the nuclei to the angular momentum of the whole molecule or mobile parts of the molecule[33,39]; and coherent "leakage", which involves the mixing of the singlet and triplet states by symmetry-breaking coherent interactions[16].

Scalar relaxation of the second kind (SR2K) is well established as a mechanism of T_1 relaxation[48,49]. This mechanism occurs when nuclei of interest have scalar couplings to additional nuclei which themselves relax rapidly. In many important cases the additional nuclei have spins $>1/2$ and their relaxation is dominated by motional modulation of the electric quadrupole coupling to local electric field gradients ("quadrupolar relaxation"). For clarity, we denote the spins whose relaxation is of primary interest by the symbol S, and the "additional nuclei" which are coupled to the spins S by the symbol I. In many cases, I and S belong to different isotopic species, but this is not necessarily the case. The relaxation of the I-spins may induce appreciable T_1 relaxation of the S-spins when the I-spin relaxation is on the timescale of the S-spin Larmor precession, i.e.:

$$\left|\omega_0^S T_1^I\right| \sim 1 \tag{1}$$

In this paper, the regime defined by Equation 1 is called the

[a)] Current address: Centre de Résonance Magnétique Nucléaire à Très Hauts Champs - FRE 2034 Université de Lyon / CNRS / Université Claude Bernard Lyon 1 / ENS de Lyon, 5 Rue de la Doua, 69100 Villeurbanne, Lyon, France
[b)] Current address: Sygnature Discovery Limited, BioCity, Pennyfoot Street, Nottingham NG1 1GF, United Kingdom
[c)] Electronic mail: mhl@soton.ac.uk

"fast fluctuation regime", where "fluctuation" refers here to the stochastic transitions between the spin states of the *S*-spins, induced by spin-lattice couplings.

In the high-field NMR of diamagnetic materials, the fast-fluctuation regime of Equation 1 is only encountered when the *I*-spin relaxation is very rapid, which normally requires a quadrupolar relaxation mechanism for the *I*-spins. The cases of ^{13}C nuclei which are scalar-coupled to ^{79}Br, ^{81}Br and ^{14}N nuclei have been studied in detail[50–54].

SR2K also relaxes the singlet order of *S*-spin pairs, in the case that the *S*-spin pair has scalar couplings to relaxing *I*-spins. Singlet relaxation by SR2K (S-SR2K) has been studied theoretically in the fast-fluctuation regime of Equation 1[55]. In this paper we discuss a second regime in which S-SR2K is active. This is the "slow fluctuation regime" of S-SR2K, which is defined as follows:

$$\left|2\pi J_{SS} T_1^I\right| \sim 1 \tag{2}$$

Here J_{SS} is the scalar coupling between the members of the *S*-spin pair which support the nuclear singlet order. This regime is encountered when the spin-lattice relaxation of the *I*-spins is on the timescale of the scalar coupling between the *S*-spins. Since this scalar coupling is typically at least 6 orders of magnitude smaller than the nuclear Larmor frequency, the regime in Equation 2 is encountered for much slower *I*-spin relaxation than for Equation 1. Indeed, the regime in Equation 2 is frequently encountered when there are finite J-couplings to nuclei with moderately short relaxation times, such as is typical for deuterium. Even spin-1/2 species such as protons may relax fast enough to satisfy Equation 2. Since deuterium substitution is often used to engineer molecules in which the spin pair has a degree of magnetic isolation from its surroundings, this is a common situation in the field of singlet NMR. The slow-fluctuation regime in Equation 2 is therefore of much practical importance.

We present a theoretical analysis of the S-SR2K mechanism in the slow-fluctuation regime for the case of spin-1/2 pairs coupled to one or more third spins. We show that in some cases the singlet-SR2K mechanism leads to strongly biexponential decay of the nuclear singlet order. Theoretical rate expressions are also presented for the case of spin-1/2 pairs coupled to single spin-1/2 nuclei exhibiting an intrinsic relaxation mechanism of their own. We show that radio-frequency (rf) irradiation which is resonant with either of the two spin species ("spin locking") can lead to a significantly reduced singlet relaxation contribution from S-SR2K and returns the decay of nuclear singlet order to a single exponential form.

We report the experimental observation of S-SR2K for $^{13}C_2$ singlet order in a solution of a [$^{13}C_2$,$^2H_2$]-labelled fumarate diester. The differential scalar couplings allow coherent access to the $^{13}C_2$ singlet order, by the SLIC (Spin-Lock Induced Crossing) radiofrequency irradiation method[18]. The singlet relaxation is found to be biexponential, as expected. The singlet relaxation time constant T_S increases with increasing ^{13}C and ^{2}H spin-locking rf field amplitudes as the S-SR2K mechanism is progressively quenched. The longest observed value of T_S approaches 30 seconds. The experimental data are compared against theoretical rate expressions.

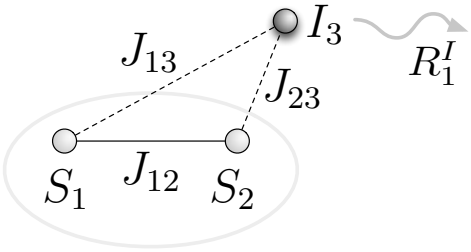

FIG. 1. Model 3-spin-1/2 system and the scalar coupling constants. The *S*-spin pair supports long-lived singlet order which is relaxed by scalar relaxation of the second kind, induced by the longitudinal relaxation of the *I*-spin with rate constant $R_1^I \sim 2\pi J_{12}$, transmitted by the differential *J*-couplings to the *S*-spin pair.

II. THEORY

A. Model spin system

Consider an ensemble of isolated spin systems, each consisting of three coupled spins-1/2. Each ensemble member contains a spin-1/2 pair, denoted S_1 and S_2, coupled to a single additional nucleus I_3, here assumed also to be spin-1/2 (see Figure 1). The couplings are assumed to be scalar (appropriate for isotropic solution) and are denoted J_{12} within each spin pair, and $\{J_{13}, J_{23}\}$ for the out of pair couplings. For simplicity, the chemical shifts of spins S_1 and S_2 are assumed to be equal, and other relaxation mechanisms acting on the *S*-spins are ignored. The third spins I_3 have relaxation mechanisms of their own, which leads to the decay rate constants $R_1^I = (T_1^I)^{-1}$ and $R_2^I = (T_2^I)^{-1}$ for *I*-spin longitudinal and transverse magnetization, respectively.

B. Liouvillian

The quantum state of the spin ensemble is described by the spin density operator ρ. Its equation of motion is the Liouville-von Neumann equation:

$$\frac{d}{dt}\rho(t) = \hat{L}(t)\rho(t) \tag{3}$$

where the Liouvillian superoperator $\hat{L}$ incorporates the coherent and incoherent influences on the spin system, and is given by:

$$\hat{L} = -i\hat{H}_{\text{coh}} + \hat{\Gamma} \tag{4}$$

where $\hat{H}_{\text{coh}}$ is the commutation superoperator of the coherent Hamiltonian H_{coh}, and $\hat{\Gamma}$ is the relaxation superoperator. Equation 3 assumes the "homogeneous" form of the master equation, but ignoring thermal corrections[56–59].

In general, the Liouvillian superoperator $\hat{L}$ has a set of $N_L = N_H^2$ eigenoperators, denoted Q_q, with $q \in \{0, 1 \ldots N_L - 1\}$, where N_H is the dimension of the Hilbert space, i.e. the number of spin states. For the ensemble of 3-spin-1/2 systems,

$N_H = 8$ and $N_L = 64$. Each Liouvillian eigenoperator has a characteristic eigenvalue, denoted Λ_q, such that:

$$\hat{L}Q_q = \Lambda_q Q_q \tag{5}$$

where in general:

$$\Lambda_q = -\lambda_q + i\omega_q \tag{6}$$

with λ_q and ω_q both being real. All eigenoperators with $\omega_q \neq 0$ correspond to coherences which decay with a rate constant λ_q and oscillate at a frequency ω_q. All eigenoperators with real eigenvalues, i.e. eigenvalues for which $\omega_q = 0$, correspond to particular configurations of spin state populations which decay with a rate constant λ_q.

The Liouvillian always has at least one trivial eigenvalue equal to zero ($\Lambda_0 = 0$) which represents the sum of populations for all states and is an invariant in a closed system. Eigenoperators with small values of the decay rate constant $\lambda_q \ll (T_1^S)^{-1}$ are called long-lived states. In the cases considered here, there is only one long-lived state, with an eigenoperator given approximately by the S-spin singlet order:

$$Q_{\mathrm{LLS}} \simeq Q_{\mathrm{SO}} = N_{\mathrm{SO}}\,\mathbf{S}_1 \cdot \mathbf{S}_2 \tag{7}$$

where $N_{SO} = -\frac{1}{2}$ is a normalization factor. This operator obeys the eigenequation:

$$\hat{L}Q_{\mathrm{LLS}} = \Lambda_{\mathrm{LLS}} Q_{\mathrm{LLS}} \tag{8}$$

with:

$$\Lambda_{\mathrm{LLS}} = -\lambda_{\mathrm{LLS}} \tag{9}$$

and $\lambda_{\mathrm{LLS}} \ll (T_1^S)^{-1}$ is the decay rate constant for the long-lived state.

A set of N_L basis operators $\mathbb{B} = \{B_0, B_1 \ldots B_{N_L-1}\}$ is said to be orthonormal if:

$$\big(B_b\big|B_c\big) = \delta_{bc} \tag{10}$$

where δ_{bc} is the Kronecker-delta, and the Liouville bracket of two operators is defined:

$$\big(A\big|B\big) = \mathrm{Tr}\{A^\dagger B\}. \tag{11}$$

A $(N_L \times N_L)$-dimensional matrix representation of the Liouvillian superoperator $\hat{L}$ in the operator basis $\mathbb{B}$ may be constructed by compiling the matrix elements:

$$\big[\hat{L}\big]^{\mathbb{B}}_{bc} = \big(B_b\big|\hat{L}\big|B_c\big) = \mathrm{Tr}\{B_b^\dagger \hat{L} B_c\}. \tag{12}$$

Diagonalization of the matrix representation $\big[\hat{L}\big]^{\mathbb{B}}$ yields the eigenoperators and eigenvalues of the Liouvillian $\hat{L}$.

1. Coherent Hamiltonian

The coherent Hamiltonian H_{coh} of the three-spin-1/2 system is conveniently written in the rotating reference frame as follows:

$$H_{\mathrm{coh}} = H_S + H_I + H_{SS} + H_{SI}. \tag{13}$$

Here the S-spin Hamiltonians are given by:

$$\begin{aligned} H_S &= \omega^S_{\mathrm{nut}}(S_x \cos\phi_S + S_y \sin\phi_S) + \Omega^S_1 S_{1z} + \Omega^S_2 S_{2z} \\ H_{SS} &= \omega_J\,\mathbf{S}_1 \cdot \mathbf{S}_2 \end{aligned} \tag{14}$$

where the in pair J-coupling is written $\omega_J = 2\pi J_{12}$, Ω^S_1 and Ω^S_2 are the chemically shifted resonance offsets of the two S-spins, relative to the S-spin reference frequency, and ω^S_{nut} represents the amplitude of the S-spin radiofrequency field, expressed as a nutation frequency. An implied sum is used for the S-spin operators, i.e. $S_x = S_{1x} + S_{2x}$. The phase of the S-spin rf field is denoted ϕ_S. Similarly, the I-spin Hamiltonian is given by:

$$H_I = \omega^I_{\mathrm{nut}}(I_x \cos\phi_I + I_y \sin\phi_I) + \Omega^I_3 I_{3z}. \tag{15}$$

The coherent Hamiltonian for the out of pair scalar couplings given by:

$$\begin{aligned} H_{SI} &= 2\pi J_{13} S_{1z} I_{3z} + 2\pi J_{23} S_{2z} I_{3z} \\ &= \frac{1}{2}(\omega_\Sigma + \omega_\Delta) S_{1z} I_{3z} + \frac{1}{2}(\omega_\Sigma - \omega_\Delta) S_{2z} I_{3z} \end{aligned} \tag{16}$$

where the sum and difference of the out of pair couplings are denoted as follows:

$$\begin{aligned} \omega_\Sigma &= 2\pi(J_{13} + J_{23}) \\ \omega_\Delta &= 2\pi(J_{13} - J_{23}). \end{aligned} \tag{17}$$

These expressions assume that the S-spins and I-spins are of different isotopic type.

2. S-spin relaxation superoperator

For simplicity, we assume that the relaxation of the S-spin system is caused by motional modulation of the dipole-dipole (DD) coupling between the two S-spins through the random tumbling of the molecules in solution. We assume the case of isotropic rotational diffusion in the extreme-narrowing limit, defined by a correlation time τ_c which is short compared to the nuclear Larmor period, i.e. $\big|\omega^0_S \tau_c\big| \ll 1$ where $\omega^0_S = -\gamma_S B^0$, γ_S is the magnetogyric ratio of the S-spins, and B^0 is the static magnetic field. This condition is often well-satisfied for small molecules in isotropic solution. In these circumstances the relaxation superoperator for S-spin relaxation is given by:

$$\hat{\Gamma}^{DD}_S \simeq -\frac{6}{5} b^2_{12} \tau_c \sum_{\mu=-2}^{+2} (-1)^\mu \hat{T}^{12}_{2\mu} \hat{T}^{12}_{2-\mu} \tag{18}$$

where the dipole-dipole coupling constant between spins S_1 and S_2 is given by:

$$b_{12} = -\frac{\mu_0}{4\pi} \gamma_S^2 \hbar r_{12}^{-3} \tag{19}$$

where r_{12} is the distance between spins S_1 and S_2 (assume to remain fixed as the molecule tumbles in solution). The symbol $\hat{T}^{12}_{2\mu}$ denotes a commutation superoperator for the second-rank

spherical tensor operator component $T^{12}_{2\mu}$. There are five such operator components, given by:

$$T^{12}_{2+2} = \frac{1}{2} S_1^+ S_2^+ \tag{20}$$

$$T^{12}_{2+1} = -\frac{1}{2}\left(S_1^+ S_{2z} + S_{1z} S_2^+\right) \tag{21}$$

$$T^{12}_{20} = \frac{1}{\sqrt{6}}\left(3 S_{1z} S_{2z} - S_1 \cdot S_2\right) \tag{22}$$

$$T^{12}_{2-1} = \frac{1}{2}\left(S_1^- S_{2z} + S_{1z} S_2^-\right) \tag{23}$$

$$T^{12}_{2-2} = \frac{1}{2} S_1^- S_2^- . \tag{24}$$

The contribution of the dipole-dipole relaxation mechanism to the spin-lattice relaxation rate constant $R_1^S = (T_1^S)^{-1}$ of the S-spins is given by:

$$(R_1^S)_{DD} = -\frac{\left(S_z \middle| \hat{\Gamma}_S^{DD} \middle| S_z\right)}{\left(S_z \middle| S_z\right)} \tag{25}$$

where the Liouville brackets are defined by Equation 11. This evaluates to:

$$(R_1^S)_{DD} = \frac{3}{2} b_{12}^2 \tau_c \tag{26}$$

in the extreme-narrowing limit.

In general, many mechanisms contribute to the S-spin relaxation, including dipole-dipole relaxation involving interactions with the I-spin, as well as chemical-shift anisotropy and spin-rotation mechanisms. For simplicity, all S-spin relaxation mechanisms other than the intra-pair dipole-dipole mechanism are ignored for now.

An important feature of the within pair DD relaxation mechanism is that it does not cause relaxation of the S-spin singlet order, when considered in isolation. This property may be expressed by the following equation:

$$(R_S)_{DD} = -\frac{\left(\mathbf{S}_1 \cdot \mathbf{S}_2 \middle| \hat{\Gamma}_S^{DD} \middle| \mathbf{S}_1 \cdot \mathbf{S}_2\right)}{\left(\mathbf{S}_1 \cdot \mathbf{S}_2 \middle| \mathbf{S}_1 \cdot \mathbf{S}_2\right)} = 0 \tag{27}$$

where R_S is the rate constant for the decay of S-spin singlet order, $R_S = (T_S)^{-1}$, and T_S is the singlet relaxation time constant. Nuclear singlet order, expressed by the operator $\mathbf{S}_1 \cdot \mathbf{S}_2$, is therefore a long-lived state which is protected from intra-pair dipole-dipole relaxation.

In practice, the DD relaxation mechanism may induce some decay of nuclear singlet order, even when other mechanisms are absent. This is because the symmetry-breaking coherent terms in the spin Hamiltonian, namely the difference in chemical shifts Ω_Δ, and the difference in J-couplings to additional spins ω_Δ, induce a mixing between the singlet and triplet states of the S-spin pair. This state mixing allows singlet order to relax through "coherent leakage" into the rapidly relaxing triplet manifold[16]. In the case where there is no chemical shift difference ($\Omega_\Delta = 0$), and the out of pair J-coupling difference is small compared to the in pair J-coupling ($|\omega_\Delta| \ll |\omega_J|$), the singlet leakage rate is given by:

$$(R_S)^{\text{leakage}}_{DD} \simeq \frac{b_{12}^2 \tau_c \omega_\Delta^2}{3 b_{12}^4 \tau_c^2 + 12 \omega_J^2} \tag{28}$$

$$\simeq \frac{R_1^S \omega_\Delta^2}{2 (R_1^S)^2 + 18 \omega_J^2} . \tag{29}$$

In cases where $\Omega_\Delta \neq 0$, Equation 29 becomes:

$$(R_S)^{\text{leakage}}_{DD} \simeq \frac{R_1^S (\omega_\Delta^2 + \Omega_\Delta^2)}{2 (R_1^S)^2 + 18 \omega_J^2} . \tag{30}$$

Equation 29 assumes that the S-spin spin-lattice relaxation rate constant R_1^S is dominated by the intra-pair dipole-dipole mechanism.

In most cases, the leakage contribution to singlet relaxation, as treated by Equation 29, is very weak. However, this expression assumes that the I-spins, to which the S-spin pair is coupled, do not themselves relax. As shown below, the I-spin relaxation can greatly increase the leakage contribution beyond that predicted by Equation 29.

3. *I-spin relaxation superoperator*

Consider the case where the I-spin, to which the S-spin pair is coupled, also undergoes relaxation. The I-spin relaxation may be treated by including a suitable relaxation superoperator $\hat{\Gamma}_I$ in the Liouvillian. For simplicity, we use here a *phenomenological* relaxation superoperator, which endows the I-spin system with a relaxation rate constant $R_1^I = (T_1^I)^{-1}$ for I-spin operators which are parallel to the external magnetic field, and a relaxation rate constant $R_2^I = (T_2^I)^{-1}$ for I-spin operators which are perpendicular to the external magnetic field. The detailed microscopic mechanisms of the I-spin relaxation are not considered at this point.

A relaxation superoperator of appropriate form is given by:

$$\hat{\Gamma}_I^{\text{phen}} = -\sum_\mu \frac{\left\{R_1^I \middle| S_\mu I_z\right)\left(S_\mu I_z\middle| + R_2^I \middle| S_\mu I_x\right)\left(S_\mu I_x\middle| + R_2^I \middle| S_\mu I_y\right)\left(S_\mu I_y\middle|\right\}}{\left(S_\mu I_z \middle| S_\mu I_z\right)} \tag{31}$$

where the sum is taken over a complete set of orthogonal S-spin operators.

The complete Liouvillian superoperator, within this simplified model of the spin system and its relaxation, is given by:

$$\hat{L} = -i\hat{H}_{\text{coh}} + \hat{\Gamma}_S^{DD} + \hat{\Gamma}_I^{\text{phen}} . \tag{32}$$

C. Case of no applied rf fields

Consider the case without the application of resonant rf fields ($\omega^I_{\text{nut}} = \omega^S_{\text{nut}} = 0$). A convenient operator basis, consisting of 64 orthonormal operators, may be defined such that the first four operators are given by:

$$\mathbb{B} = \left\{\sqrt{2} T^{12}_{00},\ -\sqrt{2} T^{12}_{20},\ (T^1_{10} - T^2_{10}) T^3_{10},\ 2\sqrt{2} T^{10}_{10},\ \ldots\right\} . \tag{33}$$

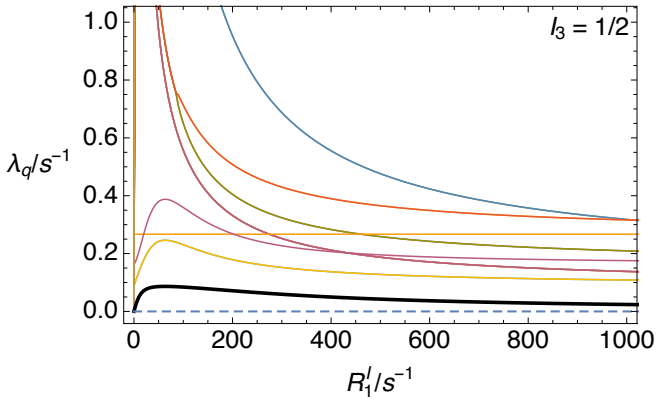

FIG. 2. Numerically determined decay rate constants λ_q for the eigenvalues of the Liouvillian superoperator in Equation 32, plotted as a function of the I-spin relaxation rate constant R_1^I. The other parameters are: $\omega_J = 2\pi \times 10\,\text{Hz}$, $\Omega_\Delta = 0$, $\omega_\Delta = 2\pi \times 2\,\text{Hz}$, $b_{12} = -2\pi \times 15\,\text{kHz}$, and $\tau_c = 20\,\text{ps}$ which corresponds to a S-spin relaxation rate constant $R_1^S = 0.267\,\text{s}^{-1}$ in the case of pure dipole-dipole relaxation. The rate constant R_1^S is visible as a horizontal orange line in the plot, corresponding to the eigenoperator S_z which has a decay rate constant independent of I-spin relaxation. The decay rate constant R_{LLS} for the long-lived state is shown by the bold line. The trivial zero eigenvalue of the unity eigenoperator is shown by the horizontal dashed line.

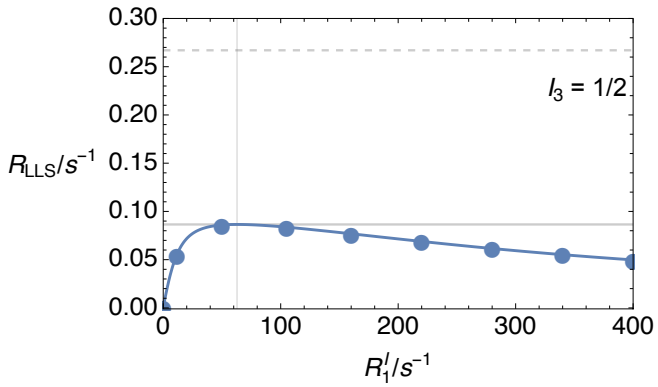

FIG. 3. Long-lived decay rate constant R_{LLS} plotted as a function of the I-spin relaxation rate constant R_1^I. The numerical results are shown by the blue points, and the analytical expression (Equation 37) by the blue line. The other parameters are: $\omega_J = 2\pi \times 10\,\text{Hz}$, $\Omega_\Delta = 0$, $\omega_\Delta = 2\pi \times 2\,\text{Hz}$, $b_{12} = -2\pi \times 15\,\text{kHz}$, and $\tau_c = 20\,\text{ps}$, corresponding to a S-spin relaxation rate constant $R_1^S = 0.267\,\text{s}^{-1}$ for pure dipole-dipole relaxation (horizontal dashed line). The rate constant R_{LLS} reaches a maximum when the I-spin relaxation rate constant matches the S-spin J-coupling, $R_1^I = \omega_J$ (vertical grey line). The maximum value of R_{LLS} is given by Equation 39 (horizontal grey line). For the case shown, this corresponds to $R_{\text{LLS}}^{\text{max}} \sim 0.32 R_1^S$.

The spherical tensor operator components are given by:

$$\begin{aligned} T_{10}^{j} &= I_{jz} \\ T_{00}^{12} &= -3^{-1/2}\,\mathbf{S}_1 \cdot \mathbf{S}_2 \\ T_{10}^{12} &= -8^{-1/2}(S_1^+ S_2^- - S_1^- S_2^+) \\ T_{20}^{12} &= 6^{-1/2}(3S_{1z}S_{2z} - \mathbf{S}_1 \cdot \mathbf{S}_2). \end{aligned} \tag{34}$$

In the absence of rf fields, the superoperator matrix representation of $\hat{L}$ is block diagonal in the basis $\mathbb{B}$, with the 4×4 block defined by the first four operators of $\mathbb{B}$ not connected by finite matrix elements to any other operators. This block is given by:

$$\left[\hat{L}\right]_{1\ldots4}^{\mathbb{B}} = \begin{pmatrix} 0 & 0 & 0 & -i\omega_\Delta/\sqrt{6} \\ 0 & -\frac{9}{10}b_{12}^2\tau_c & 0 & i\omega_\Delta/2\sqrt{3} \\ 0 & 0 & -R_1^I - \frac{1}{2}b_{12}^2\tau_c & -i\omega_J \\ -i\omega_\Delta/\sqrt{6} & i\omega_\Delta/2\sqrt{3} & -i\omega_J & -R_1^I - \frac{1}{2}b_{12}^2\tau_c \end{pmatrix}. \tag{35}$$

Assuming that the S-spin relaxation is dominated by the intra-pair dipole-dipole mechanism, this may be written as:

$$\left[\hat{L}\right]_{1\ldots4}^{\mathbb{B}} \simeq \begin{pmatrix} 0 & 0 & 0 & -i\omega_\Delta/\sqrt{6} \\ 0 & -\frac{3}{5}R_1^S & 0 & i\omega_\Delta/2\sqrt{3} \\ 0 & 0 & -R_1^I - \frac{1}{3}R_1^S & -i\omega_J \\ -i\omega_\Delta/\sqrt{6} & i\omega_\Delta/2\sqrt{3} & -i\omega_J & -R_1^I - \frac{1}{3}R_1^S \end{pmatrix}. \tag{36}$$

This matrix has four complex eigenvalues. The decay rate constant of the long-lived state is given by minus the smallest negative eigenvalue (see equation 9). The rate constants λq for the decay of eigenoperators Q_q, with $q \in \{0\ldots63\}$, may be derived from the matrix representation of $\hat{L}$ in the basis $\mathbb{B}$, as described in equations 5 to 6. These rate constants are plotted against the I-spin relaxation rate constant R_1^I for a typical set of parameters in Figure 2. Numerical simulations were performed by using the *Mathematica*-based NMR software package *SpinDynamica*[60]. The colouring of the different eigenvalue curves is arbitrary. Apart from the trivial eigenvalue $\lambda_0 = 0$ (horizontal dashed line), which belongs to the unity eigenoperator and which represents the conserved sum of all state populations, the smallest rate constant (bold line) corresponds to the decay rate constant R_{LLS} for the long-lived mode of S-spin singlet order.

It has not proved possible to obtain a compact exact form for this rate constant. However, an approximate analytical result may be obtained by deploying Primas-van Vleck perturbation theory[61–65]. The method is described in the Appendix, and leads to the following expression:

$$R_{\text{LLS}} \simeq \frac{3R_1^S}{10} + \frac{R_1^I\omega_\Delta^2}{8\rho^2} - \frac{1}{40}\sqrt{144(R_1^S)^2 - \frac{40R_1^S R_1^I \omega_\Delta^2}{\rho^2} + \frac{25(R_1^I)^2\omega_\Delta^4}{\rho^4}} \tag{37}$$

where:

$$\rho^2 = (R_1^I)^2 + \omega_J^2 \tag{38}$$

For the typical parameters, this expression yields values which are indistinguishable from the numerical results (Figure 3). Equation 37 shows that a finite relaxation rate constant R_1^I for the I-spin augments the relaxation rate constant R_{LLS} for the long-lived state by mixing in a dependence on the S-spin relaxation rate R_1^S. In other words, the leakage mechanism for long-lived state decay is augmented by the relaxation of the I-spin. This is the essence of the S-SR2K mechanism.

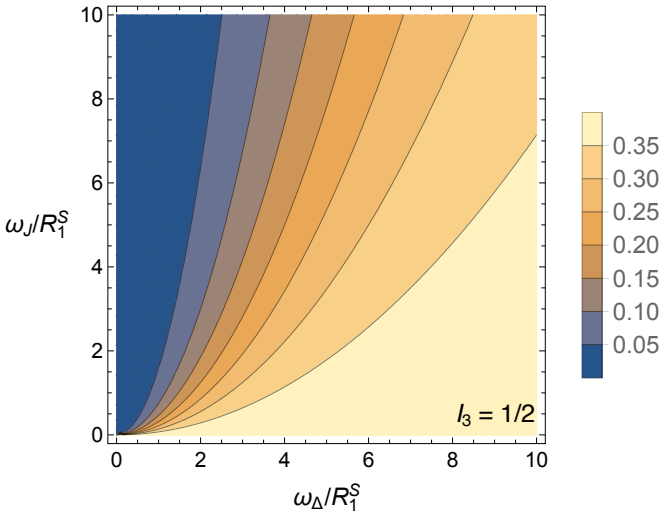

FIG. 4. Contour plot of $R_{\mathrm{LLS}}^{\mathrm{max}}/R_1^S$ against the coupling parameters ω_Δ and ω_J. At each point on the plot, the I-spin relaxation rate constant R_1^I is set to the J-coupling ω_J, in order to induce the fastest possible SR2K contribution to the long-lived state relaxation. The plot indicates the regions of parameter space which are well-protected against the SR2K mechanism of long-lived state relaxation (dark blue), and the regions where, in the worst case, SR2K leakage induced by a single spin-1/2 may restrict the lifetime of the long-lived state to about $3T_1^S$ (yellow).

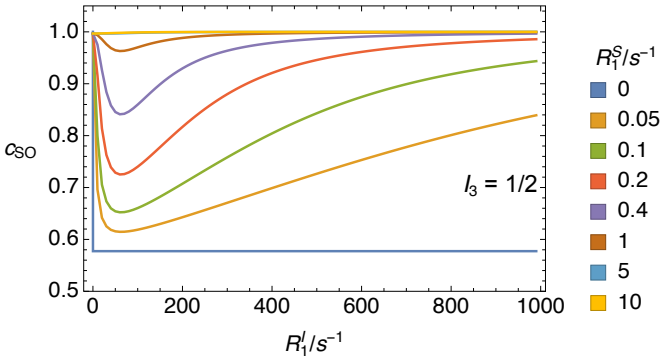

FIG. 5. Coefficient c_{SO} of singlet order in the long-lived eigenoperator Q_{LLS} as a function of the rate constant R_1^I, for several different values of the rate constant R_S^I, assuming pure dipole-dipole relaxation for the S-spins. The other parameters are: $\omega_J = 2\pi \times 10\,\mathrm{Hz}$, $\Omega_\Delta = 0$, and $\omega_\Delta = 2\pi \times 2\,\mathrm{Hz}$. The long-lived eigenoperator approximates singlet order when there is no I-spin relaxation ($R_1^I = 0$) and when the S-spin relaxation is rapid. In the extreme case of no S-spin relaxation but finite I-spin relaxation, the long-lived eigenoperator is given by "zz-order", not singlet order. The singlet order coefficient is $c_{\mathrm{SO}} = 1/\sqrt{3}$ in this case (shown by the blue line).

A plot of the relaxation rate constant R_{LLS} against the I-spin relaxation rate constant R_1^I is shown for typical parameters in Figure 3. When $R_1^I = 0$ the long-lived relaxation rate R_{LLS} is very small and given by the coherent leakage term (see Equation 29). However, the long-lived relaxation rate rapidly increases as R_1^I increases. A maximum in R_{LLS} is achieved when the I-spin relaxation rate constant matches the J-coupling between the S-spins, $R_1^I = \omega_J$ (indicated by the vertical grey line in Figure 3). The relaxation rate of the long-lived state decreases slowly as R_1^I increases beyond ω_J.

The behaviour has the following physical interpretation: The longitudinal relaxation processes of the I-spin cause fluctuations in the local magnetic field at the site of the S-spins, as transmitted by the heteronuclear J-couplings. If the J-couplings are different ($\omega_\Delta \neq 0$), the local field fluctuations induce singlet-triplet transitions, allowing singlet order to leak into the more rapidly relaxing triplet manifold. Since the energy difference between the singlet and central triplet states of the S-spins corresponds to ω_J in frequency units, the effect is strongest when the I-spin relaxation rate R_1^I matches the J-coupling ω_J.

The maximum rate of long-lived state relaxation, induced by the SR2K mechanism, is given by evaluating Equation 37 at the condition $R_1^I = \omega_J$ which leads to the following expression:

$$R_{\mathrm{LLS}}^{\mathrm{max}} \simeq \frac{3R_1^S}{10} + \frac{\omega_\Delta^2}{16\omega_J} - \frac{1}{40}\sqrt{144(R_1^S)^2 - \frac{20R_1^S\omega_\Delta^2}{\omega_J} + \frac{25\omega_\Delta^4}{4\omega_J^2}}. \tag{39}$$

The value of $R_{\mathrm{LLS}}^{\mathrm{max}}$ is shown by the horizontal grey line in Figure 3. For the parameters shown, the "worst case" ratio of the long-lived state relaxation rate constant R_{LLS} to the longitudinal relaxation rate constant R_1^S is ~ 0.32, i.e. the long-lived state decays only about 3 times slower than the longitudinal magnetization.

Figure 4 shows a contour plot of the "worst case" ratio of the long-lived and longitudinal S-spin relaxation rate constants, $R_{\mathrm{LLS}}^{\mathrm{max}}/R_1^S$, as a function of the two coupling parameters ω_Δ and ω_J, which are also expressed as ratios of R_1^S. The blue shading indicates the region of parameter space where the long-lived state is well-protected against the SR2K mechanism. This requires that the heteronuclear difference frequency ω_Δ is not too large (less than roughly twice the S-spin relaxation rate constant R_1^S), and the S-spin J-coupling ω_J is not too small (at least R_1^S). In this region, the maximum value of the long-lived state decay time constant T_{LLS}, taking into account the SR2K mechanism alone, is at least 20 times T_1. In the very worst case, on the other hand, where ω_Δ is large and ω_J is small, the SR2K mechanism induced by a single I-spin-1/2 may give rise to a long-lived-state relaxation rate constant $R_{\mathrm{LLS}} = (2/5)R_1^S$, i.e. the ratio of T_{LLS} to T_1 is not larger than 2.5.

Although Figure 4 represents the "worst case" scenario, in which the I-spin relaxation rate constant is always chosen to give the fastest possible leakage, this plot indicates that the SR2K mechanism of long-lived state relaxation is likely to be commonly encountered. It may be no coincidence that a time constant ratio of $T_{\mathrm{LLS}}/T_1 \sim 3$ is frequently encountered in practice, unless special precautions are taken.

We now consider the nature of the long-lived state, i.e. the eigenoperator Q_{LLS} with eigenvalue $\Lambda_{\mathrm{LLS}} = -R_{\mathrm{LLS}}$. In many regions of parameter space, this eigenoperator corresponds closely to the singlet order operator T_{00}^{12} of Equation 34. How-

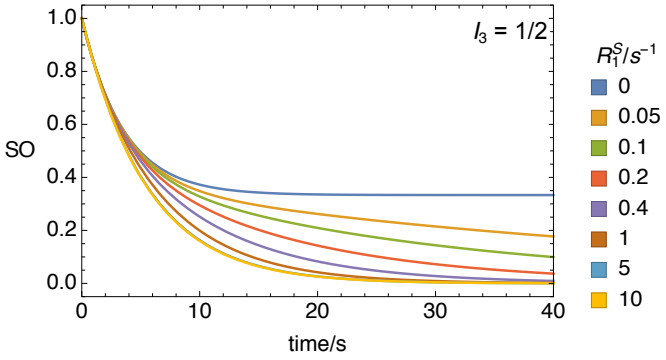

FIG. 6. Simulated trajectories of S-spin singlet order in time, for the indicated values of the S-spin relaxation rate constant R_1^S, assuming pure dipole-dipole relaxation for the S-spins. The other parameters are: $\omega_J = 2\pi \times 10\,\text{Hz}$, $\Omega_\Delta = 0$, $\omega_\Delta = 2\pi \times 2\,\text{Hz}$, and $R_1^I = 100\,\text{s}^{-1}$. The decay of singlet order is non-monoexponential in the regime where $c_{SO} < 1$ (see Figure 5). In the case of $R_1^S = 0$, the singlet order projects onto zz-order at long times rather than decaying to zero.

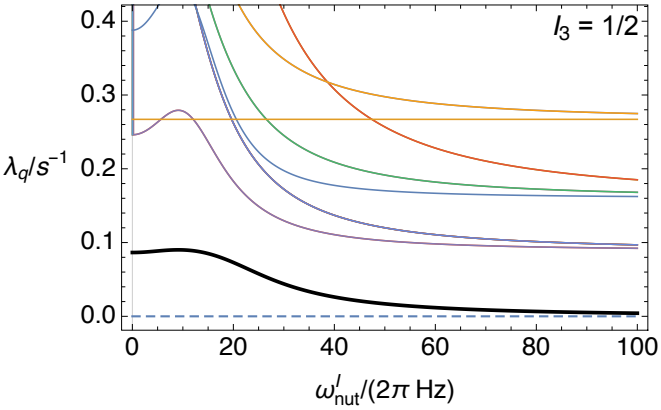

FIG. 7. Eigenoperator decay rate constants as a function of rf field amplitude on the I-spins, expressed as a nutation frequency ω_{nut}^I. The other parameters are: $R_1^I = \omega_J = 2\pi \times 10\,\text{Hz}$, $\Omega_\Delta = 0$, $\omega_\Delta = 2\pi \times 2\,\text{Hz}$, $R_1^S = 0.267\,\text{s}^{-1}$. The condition $R_1^I = \omega_J$ maximizes the SR2K effect. Pure S-spin dipole-dipole relaxation is assumed. The decay rate constant of the long-lived state is shown in bold. Strong I-spin rf fields suppress the SR2K decay mechanism.

ever, this is not always the case. The coefficient of singlet order in the long-lived eigenoperator Q_{LLS} is given by:

$$c_{SO} = \left(\sqrt{2}T_{00}^{12} \middle| Q_{LLS}\right) \tag{40}$$

with the Liouville bracket defined by Equation 11. A coefficient $c_{SO} = 1$ indicates that the long-lived state is pure singlet order; a coefficient $c_{SO} < 1$ indicates that the long-lived state consists of singlet order mixed with other operators. Figure 5 shows plots of the coefficient c_{SO} for the long-lived eigenstate as a function of the relaxation rate constant R_1^I, for various values of the rate constant R_1^S, assuming pure dipole-dipole relaxation for the S-spins. These plots show that the long-lived state corresponds to nearly pure singlet order in the case of no I-spin relaxation ($R_1^I = 0$) and relatively rapid S-spin relaxation. However, in other cases, the long-lived state consists of a mixture of singlet order with other operators. The admixture of other operators is maximal near the condition $R_1^I = \omega_J$, where singlet-SR2K is most significant.

In the extreme case of $R_1^S = 0$ (no S-spin relaxation), but finite I-spin relaxation, the long-lived state corresponds to the operator $\sqrt{2}S_{1z}S_{2z}$, i.e. "zz-order", rather than singlet order (blue line in Figure 5). In this case the singlet-order coefficient in the LLS is given by:

$$c_{SO} = \left(\sqrt{2}T_{00}^{12} \middle| \sqrt{2}S_{1z}S_{2z}\right) = \frac{1}{\sqrt{3}} = 0.578 \tag{41}$$

for all $R_1^I > 0$. The physical interpretation of this is as follows: the singlet order operator may be expressed:

$$\sqrt{2}T_{00}^{12} = -\sqrt{\frac{2}{3}}S_{1z}S_{2z} - \frac{1}{\sqrt{6}}(S_1^+S_2^- + S_1^-S_2^+). \tag{42}$$

If the I-spin has significant relaxation, and there is no S-spin relaxation, the second term (the "flip-flop" term) dephases under the SR2K effects, while the first term (the "zz" term) remains invariant. However, the isolation of these two terms is disrupted if there is significant S-spin relaxation, in which case the singlet order takes over its usual role as the long-lived eigenoperator.

The relaxation of S-spin singlet order is non-monoexponential in the regime where the coefficient c_{SO} is significantly less than 1. Figure 6 shows simulated trajectories of the decay of singlet order in the presence of SR2K effects for various values of the S-spin relaxation rate constant R_1^S. In the extreme case of $R_1^S = 0$, the "zz" part of the singlet order does not decay at all (blue line). Note that increasingly large values of R_1^S do not induce more rapid singlet relaxation: the main effect of increasing R_1^S is merely to reduce the biexponentiality of the relaxation trajectory.

D. SR2K suppression by resonant rf fields

The effect of SR2K on the relaxation of the long-lived state is strongly influenced by the application of resonant radiofrequency fields. The resonant fields may be applied to either the I-spins or the S-spins.

1. *I-spin rf fields*

The effect of a resonant I-spin field may be explored by numerical simulations of the Liouvillian eigenvalues, including a finite value of ω_{nut}^I in Equation 15. The decay rate constants λ_q of the Liouvillian eigenoperators are plotted against the rf field amplitude on the I-spins, expressed as a nutation frequency ω_{nut}^I, in Figure 7. In this case the I-spin relaxation rate constant R_1^I is matched to the S-spin J-coupling ω_J, which maximises the SR2K effect in the absence of rf fields. The decay rate constant of the long-lived state is shown by the bold

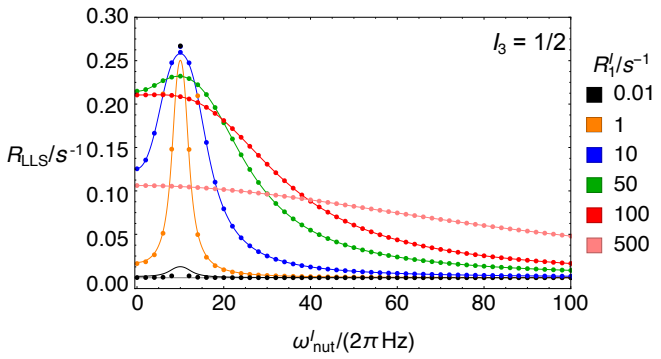

FIG. 8. Decay rate constant λ_{LLS} for the long-lived state as a function of rf field amplitude on the I-spins, expressed as a nutation frequency ω^I_{nut}, for different values of the I-spin relaxation rate constant R^I_1. The other parameters are: $\omega_J = 2\pi \times 10\,Hz$, $\Omega_\Delta = 0$, $\omega_\Delta = 2\pi \times 2\,Hz$, $R^S_1 = 0.267\,s^{-1}$. Pure S-spin dipole-dipole relaxation is assumed. The decay of the long-lived state is accelerated by the application of small I-spin rf fields, especially when the I-spin relaxation rate constant R^I_1 is small. Strong I-spin rf fields suppress the SR2K-induced decay in all cases. The values of the approximate analytical expression in Equation 43 are shown by the dots.

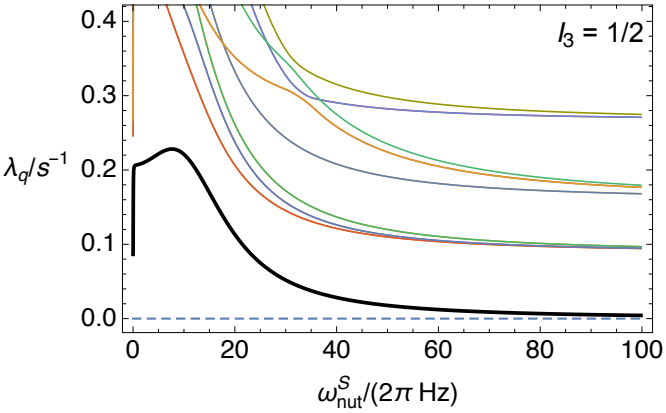

FIG. 9. Eigenoperator decay rate constants as a function of rf field amplitude on the S-spins, expressed as a nutation frequency ω^S_{nut}. The other parameters are: $R^I_1 = \omega_J = 2\pi \times 10\,Hz$, $\Omega_\Delta = 0$, $\omega_\Delta = 2\pi \times 2\,Hz$ and $R^S_1 = 0.267\,s^{-1}$. Pure S-spin dipole-dipole relaxation is assumed. The condition $R^I_1 = \omega_J$ maximizes the SR2K effect. The decay rate constant of the long-lived state is shown in bold. The application of an S-spin rf field enhances the SR2K decay mechanism at small values of ω^S_{nut}, but suppresses SR2K at large rf field amplitudes. A detailed view of the low rf field regime is shown in Figure 10.

line. The application of strong I-spin rf fields suppresses the SR2K-induced decay of the long-lived state.

The dependence of λ_{LLS} on the I-spin rf field amplitude is explored for a range of values of the rate constant R^I_1 in Figure 8. Two regimes may be identified: When the I-spin relaxation is slow ($R^I_1 < |\omega_J|$), a strong increase in the decay rate of the LLS is observed when the I-spin rf field amplitude matches the condition $\omega^I_{nut} = \omega_J$. This is a variant of the spin-lock-induced-crossing (SLIC) condition[18]. When the I-spin relaxation is rapid ($R^I_1 < |\omega_J|$), the application of a small I-spin rf field has little effect. In all cases, an applied rf field with amplitude $\omega^I_{nut} > \omega_J$ suppresses the SR2K-induced decay of the long-lived state. However, the effect is small when the I-spin has very rapid I-spin relaxation.

An approximate analytical expression for λ_{LLS} has been obtained in the near magnetic equivalence regime, $|\omega_J| \gg |\omega_\Delta|$, and the limit of a strong I-spin rf field, $|\omega^I_{nut}| \gg |\omega_\Delta|$, and assuming $R^I_1 = R^I_2$. The derivation is given in the appendix. This expression is as follows:

$$R_{LLS}(\omega^I_{nut}) \simeq \frac{3R^S_1}{10} + \frac{A}{8D} - \frac{9}{20}\sqrt{\frac{4(R^S_1)^2}{9} - \frac{5}{324}\frac{(8R^S_1 ABC - A)}{D^2}} \tag{43}$$

where the following abbreviations have been used:

$$A = R^I_1\omega^2_\Delta(\omega^2_{nut} + \omega^2_J + (R^I_1)^2) \tag{44}$$
$$B = (R^I_1)^2 + (\omega^2_{nut} - \omega^2_J)^2 \tag{45}$$
$$C = (R^I_1)^2 + (\omega^2_{nut} + \omega^2_J)^2 \tag{46}$$
$$D = (R^I_1)^4 + (\omega^2_{nut} - \omega^2_J)^2 + 2R^I_1(\omega^2_{nut} + \omega^2_J). \tag{47}$$

The values of Equation 43 are shown by the dots in Figure 8 and agree well with the numerical results (except for a single point on the line with $R^I_1 = 0.01\,s^{-1}$ at $\omega^1_{nut}/2\pi = 10\,Hz$).

2. *S-spin rf fields*

The SR2K mechanism of long-lived-state decay is also strongly influenced by radiofrequency fields resonant with the S-spin pair.

The decay rate constants of the Liouvillian eigenoperators are plotted against the rf field amplitude on the S-spins, expressed as a nutation frequency ω^S_{nut}, in Figure 9. In this simulation, the I-spin relaxation rate constant R^I_1 is matched to the S-spin J-coupling ω_J, which maximises the SR2K effect in the absence of rf fields. The decay rate constant of the long-lived state is shown by the bold line. The application of a very small S-spin rf field sharply increases the decay rate constant λ_{LLS}. A further increase in the S-spin field amplitude first accelerates the decay rate of the long-lived state, until a maximum decay rate is reached at around $\omega^S_{nut} \simeq \omega_J$. Further increase of the rf field amplitude sharply decreases the relaxation rate constant, indicating the suppression of the SR2K mechanism.

The sharp increase in the rate constant λ_{LLS} at very small values of ω^S_{nut} is remarkable. This regime is explored in more detail in Figure 10. This shows clearly the increase in the decay rate constant of the long-lived state when very small S-spin fields are applied, accompanied by complex branching and merging of the other Liouvillian eigenvalues.

This behaviour may be understood qualitatively as follows: In the case of significant I-spin relaxation, and no S-spin relaxation, the "zz" component of S-spin singlet order is longer lived than the "flip-flop" component, since the latter is dephased by the rapid I-spin relaxation (see Equation 42 and subsequent discussion). The long-lived eigenoperator in the absence of an S-spin rf field is therefore close to "zz" order for the S-spins (see Figure 5). This situation corresponds to

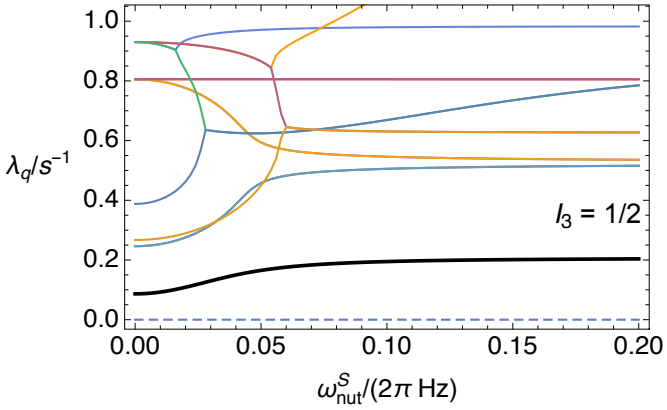

FIG. 10. Detail of Figure 9 at small values of ω^S_{nut}. This shows the increase in the decay rate constant of the LLS when very weak S-spin rf fields are applied, and the complex behaviour of the other eigenvalues in this regime.

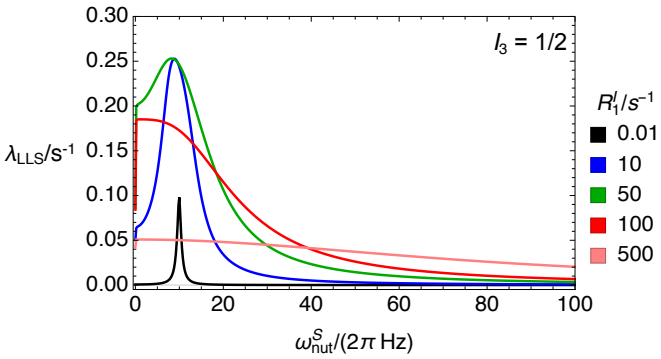

FIG. 11. Decay rate constant λ_{LLS} for the long-lived state as a function of rf field amplitude on the S-spins, expressed as a nutation frequency ω^S_{nut}, for different values of the I-spin relaxation rate constant R^I_1. The other parameters are: $\omega_I = 2\pi \times 10\,\text{Hz}$, $\Omega_\Delta = 0$, $\omega_\Delta = 2\pi \times 2\,\text{Hz}$, $R^S_1 = 0.267\,\text{s}^{-1}$. Pure S-spin dipole-dipole relaxation is assumed. The prominent feature at $\omega^S_{nut} = \omega_I$, which appears for small values of R^I_1, corresponds to the SLIC (spin-lock-induced-crossing) condition. This feature is suppressed for large values of R^I_1. The decay of the long-lived state is accelerated by the application of small S-spin rf fields, when R^I_1 is small. Large S-spin rf fields suppress the SR2K-induced decay, although the effect of the rf field becomes marginal when the I-spin relaxation rate constant R^I_1 is large.

the left-hand edges of the plots in Figures 9 and 10. The application of a very weak S-spin rf field is enough to mix the slowly relaxing "zz" component of S-spin singlet order with the more rapidly relaxing "flip-flip" component. This leads to a significant increase in the relaxation rate constant of the long-lived state, as shown clearly by the bold lines in Figures 9 and 10. The relaxation rate constant of the long-lived state comes down again when the S-spin rf field amplitude is large enough to average out the heteronuclear J-couplings which underly the SR2K phenomenon (see Figure 9).

The dependence of λ_{LLS} on the S-spin rf field amplitude is explored for a range of values of the rate constant R^I_1 in Figure 11. As in the case of I-spin rf fields (Figure 8), two regimes may be identified. When the I-spin relaxation is slow ($R^I_1 < |\omega_I|$), a prominent feature appears when the S-spin rf field matches the *intra*-pair J-coupling ($\omega^S_{nut} = \omega_I$). This corresponds to the spin-lock-induced-crossing (SLIC) condition[18]. This feature disappears in the case of rapid I-spin relaxation ($R^I_1 \geq |\omega_I|$). The application of strong S-spin rf fields suppresses the relaxation of the long-lived state in all cases. However, the effect of strong S-spin rf fields becomes marginal when the I-spin relaxation is very rapid.

Strong S-spin rf fields are more effective in suppressing SR2K than strong I-spin rf fields, at the same nutation frequency (compare Figure 8 and Figure 11).

It has not yet been possible to obtain an analytical result for the decay rate constant λ_{LLS} as a function of the rf field amplitude applied to the S-spins.

E. The case of a quadrupolar I-spin

Consider the case where the additional nucleus I_3 is spin-1, such that the isolated three spin system in the ensemble consists of a spin-1/2 pair and a quadrupolar nucleus. The I-spin possesses a dominant quadrupolar relaxation mechanism due to the coupling interaction between the intrinsic electric quadrupole moment and the local electric field gradient (EFG) being motionally modulated by the random tumbling of the molecules in solution. We assume, for simplicity, that the relaxation mechanism of the I-spin is not cross-correlated with the in pair dipole-dipole relaxation mechanism of the S-spins.

For the case of isotropic tumbling in the extreme-narrowing limit, the quadrupolar relaxation superoperator for the I-spin is given by:

$$\hat{\Gamma}^Q_I \simeq -\frac{3}{10}\omega^2_Q \tau_c \sum_{\mu=-2}^{+2} (-1)^\mu \hat{T}^3_{2\mu}\hat{T}^3_{2-\mu} \tag{48}$$

where the quadrupolar coupling constant of the spin-1 nucleus I_3 is given by:

$$\omega_Q = \frac{e^2 qQ}{2\hbar} \tag{49}$$

where Q is the electric quadrupolar moment of the quadrupolar nucleus, and eq is the electrical field gradient at the quadrupolar nucleus[66]. The five operator components $\hat{T}^3_{2\mu}$ are given by:

$$T^3_{2+2} = \frac{1}{2}(I^+_3)^2 \tag{50}$$

$$T^3_{2+1} = -\frac{1}{2}\left(I^+_3 I_{3z} + I_{3z} I^+_3\right) \tag{51}$$

$$T^3_{20} = \frac{1}{\sqrt{6}}\left(3I^2_{3z} - I_3(I_3+1)\right) \tag{52}$$

$$T^3_{2-1} = \frac{1}{2}\left(I^-_3 I_{3z} + I_{3z} I^-_3\right) \tag{53}$$

$$T^3_{2-2} = \frac{1}{2}(I^-_3)^2 \tag{54}$$

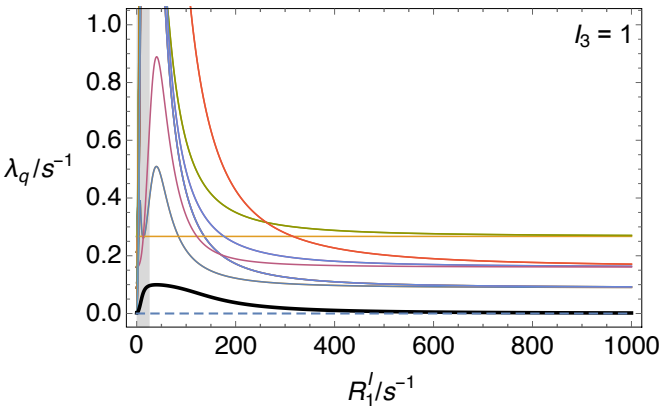

FIG. 12. Numerically determined decay rate constants λ_q for the eigenvalues of the Liouvillian superoperator in Equation 56, plotted as a function of the I-spin relaxation rate constant R_1^I, in the case that the I_3 is spin-1. The other parameters are: $\omega_I = 2\pi \times 10\,\text{Hz}$, $\Omega_\Delta = 0$, $\omega_\Delta = 2\pi \times 2\,\text{Hz}$, $b_{12} = -2\pi \times 15\,\text{kHz}$, and $\tau_c = 20\,\text{ps}$ which corresponds to a S-spin relaxation rate constant $R_1^S = 0.267\,\text{s}^{-1}$ in the case of pure dipole-dipole relaxation. The decay rate constant R_{LLS} for the long-lived state is shown by the bold line. The trivial zero eigenvalue of the unity eigenoperator is shown by the horizontal dashed line. The grey region shows the typical range of parameters for deuterium sites in small molecules.

The quadrupolar relaxation mechanism is the dominant decay process contributing to the longitudinal relaxation rate constant $R_1^I = (T_1^I)^{-1}$ of the I-spin, and is given by:

$$R_1^I = -\frac{\left(I_z\middle|\hat{\Gamma}_I^Q\middle|I_z\right)}{\left(I_z\middle|I_z\right)} = \frac{3}{2}\omega_Q^2\tau_c \tag{55}$$

for the case that I_3 is spin-1. In this instance, the complete Liouvillian superoperator is given by:

$$\hat{L} = -i\hat{H}_{\text{coh}} + \hat{\Gamma}_S^{DD} + \hat{\Gamma}_I^{\text{Q}}. \tag{56}$$

A numerical analysis of the Liouvillian eigenvalues λ_Q, plotted against the quadrupolar relaxation rate constant R_1^I of the spin $I_3 = 1$, is shown in Figure 12. All parameters are identical to those in section II C, with the exception that the I-spin relaxation uses the semi-classical quadrupolar relaxation superoperator in Equation 48. The maximum SR2K relaxation rate constant is found to be ∼15% higher than the case of $I_3 = 1/2$. An analytical expression for the singlet rate constant in this case has not been found.

The grey region of Figure 12 denotes the typical range of quadrupolar spin-lattice relaxation rate constants for deuterium nuclei covalently attached to small organic molecules dissolved in solution. The shaded area coincides with the region of maximal singlet relaxation (bold line), demonstrating that deuterium nuclei can provide a significant relaxation source for the singlet order of the spin-1/2 pair.

For the case of a quadrupolar I-spin, the biexponential nature of the long-lived state and its behaviour under the application of on resonant I-spin and S-spin radiofrequency fields are detailed in the Supplementary Material (SM).

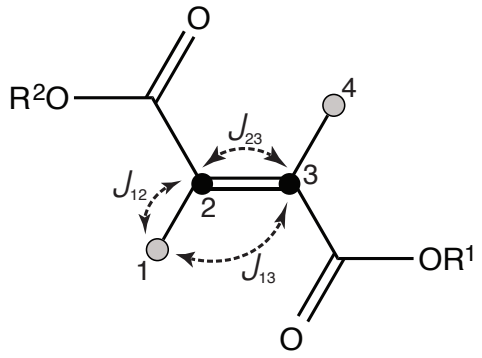

FIG. 13. Molecular structure, labelling scheme and scalar coupling constant pattern of **I**. Black circles denote ^{13}C nuclei, grey circles denote ^{2}H nuclei. $R^1 = CD_2CD_3$ and $R^2 = CD_2CD_2CD_3$.

III. EXPERIMENTS

A. Experimental methods

It proved difficult to identify a test molecular system containing a thee-spin system with appropriate properties. We therefore studied the perdeuterated ethyl/propyl diester of 2,3-$^{13}C_2$-fumarate (1-(ethyl-d_5) 4-(propyl-d_7)(*E*)-but-2-enedioate-2,3-$^{13}C_2$-d_2, **I**) (see Figure 13). This molecule contains a 4-spin system of two ^{13}C nuclei and ^{2}H nuclei, which displays the same essential spin physics as the 3-spin systems discussed above.

21 mg of **I** was dissolved in 0.5 mL of $CDCl_3$ solvent at a concentration of 0.207 M. Samples were subjected to thorough degassing using 6 standard freeze-pump-thaw cycles in a Wilmad low pressure/vacuum NMR tube (5 mm outer diameter) to remove the majority of dissolved molecular oxygen in solution. Details of the chemical synthesis are given in the Supplementary Material (SM).

The material **I** contains a central spin system comprised of two ^{13}C nuclei and two ^{2}H nuclei over a *trans*-double bond. The 2-spin-1/2,2-spin-1 system displays a local centre of inversion, midway between the two ^{13}C nuclei. The asymmetric ester groups R^1 and R^2 provide a small chemical shift difference between the ^{13}C nuclei and are deuterated in order to reduce their relaxation contribution from intramolecular dipole-dipole couplings. Note that we did not exploit the small chemical shift difference between the ^{13}C nuclei in the current study.

B. ^{13}C NMR

The relevant portion of the experimental ^{13}C NMR spectrum of **I** is shown in Figure 14. The chemical shift of the $^{13}C_2$ resonance was referenced with respect to the $CDCl_3$ solvent peak = 77.2 ppm.

The experimental ^{13}C NMR spectrum of **I** was fitted using the *MatLab*-based NMR software package *Spinach*[67]. The fitted scalar couplings and chemical shifts (including their differences) for **I** in $CDCl_3$ solvent at 25°C are given in Table I.

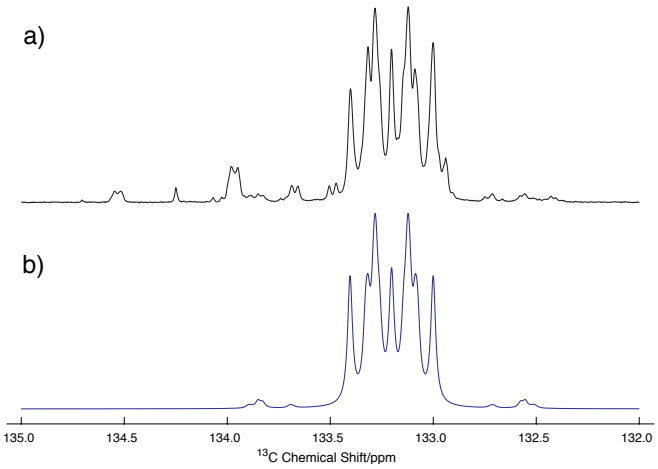

FIG. 14. Relevant portion of the experimental ^{13}C NMR spectrum of **I** dissolved in degassed $CDCl_3$ solution acquired at 11.75 T (^{13}C nuclear Larmor frequency = 125.8 MHz) and 25°C with 64 transients. Black curve: experimental ^{13}C spectrum; blue curve: simulated ^{13}C spectrum. Small signals from synthetic impurities are observed beyond 133.5 ppm.

The spin system is in the near-equivalence regime, since the difference in scalar couplings $|J_{12}-J_{13}|$ is less than half of J_{23}.

The ^{13}C longitudinal relaxation time $T_1(^{13}\mathrm{C})$ was estimated experimentally by using the inversion-recovery pulse sequence. Under the same conditions, the resulting relaxation curve (see the Supplementary Material (SM)) shows a single exponential recovery with a longitudinal ^{13}C relaxation time: $T_1(^{13}\mathrm{C}) = 14.0 \pm 0.5$ s.

C. Deuterium NMR

The ^{2}H spectrum of **I** is shown in the Supplementary Material (SM). The longitudinal ^{2}H relaxation time $T_1(^2\mathrm{H})$ was estimated experimentally by using the inversion recovery pulse sequence. For the case of degassed $CDCl_3$ solution at 11.7 T and 25°C, the experimental relaxation curve (see the Supplementary Material (SM)) shows a single exponential recovery with a longitudinal ^{2}H relaxation time: $T_1(^2\mathrm{H}) = 168 \pm 7$ ms.

D. Singlet NMR

Symmetry-breaking interactions, such as small differences in chemical shift between the participating spins, or differential scalar couplings to other magnetic nuclei outside of the singlet pair are required for coherent access to the nuclear singlet order[14]. In this case, the differential out-of-pair scalar couplings allow coherent access to the ^{13}C nuclear singlet order of **I**, by using known radiofrequency pulse techniques which operate in the near-equivalence regime[10,13,18,22], as shown by Warren and coworkers[14,26,35]. In the current study, the spin-lock induced crossing (SLIC) pulsed method[18] was used, as shown in Figure 15. Details of the SLIC pulse sequence, parameter optimization and the "T_{00} filter" are found in the Supplementary Material (SM). The parameters of the SLIC pulse were chosen to maximise triplet-singlet population conversion: $\omega_{\mathrm{SLIC}}/2\pi$ = 71.5 Hz and τ_{SLIC} = 27 ms, i.e. the conversion was complete in a time: $\tau_{\mathrm{SLIC}} \simeq 2^{-1/2}(|J_{12}-J_{13}|)^{-1}$. The maximum amplitude of the singlet-filtered ^{13}C NMR signal, relative to that induced by a single 90° pulse, was found to be 0.067. The loss relative to the theoretical maximum of 1/3 (AA′XX′ spin systems) is not yet fully understood. The parameters used for this pulse sequence are such that the generation of $^{13}C_2$ singlet order takes place predominantly through the differential ^{13}C-^{2}H couplings, with the small chemical shift difference between the ^{13}C nuclei playing a negligible role.

TABLE I. Spin system parameters for **I** in $CDCl_3$ solvent at 25°C. Labels 2 and 3 indicate ^{13}C nuclei, labels 1 and 4 indicate ^{2}H nuclei. Scalar couplings and chemical shifts (including their differences) were obtained by fitting the experimental ^{13}C NMR spectrum with the *MatLab*-based NMR software package *Spinach*[67]. The ^{13}C chemical shift frequency difference at 11.75 T is given by $\Delta\Omega^S_{23} = \Omega^S_2 - \Omega^S_3$.

Parameter	Value/Hz
J_{23}	71.5 ± 0.9
$J_{12} = J_{34}$	25.9 ± 0.3
$J_{13} = J_{24}$	-0.5 ± 0.1
$\lvert J_{12} - J_{13}\rvert$	26.4 ± 0.3
$\Delta\Omega^S_{23}/2\pi$	7.75 ± 0.05

IV. RESULTS

A. Singlet order decay in the absence of rf fields

A decay curve for the ^{13}C signal intensity of **I** under the pulse sequence shown in Figure 15 is shown in Figure 16. The experimental decay (black data points) is well fitted with a biexponential decay function of the form: A exp{-t/T_A} + B exp{-t/T_B} (black curve). The fit parameters are: A = 0.772, $T_A = 240 \pm 40$ ms, B = 0.504, $T_B = 3.6 \pm 0.3$ s. Note that the decay is much faster than that of longitudinal ^{13}C magnetization ($T_1(^{13}\mathrm{C}) = 14.0$ s). The rapid quenching of nuclear singlet order, and the biexponential decay, support a strong role for SR2K as a singlet relaxation mechanism in this system.

Numerical simulation of the long-lived state relaxation dynamics requires an estimate of the rotational correlation time τ_c. This was estimated by analyzing the experimental relaxation time constant R^I_1 for the ^{2}H nuclei adjacent to the ^{13}C spin pair, using Equation 55 which applies for extreme-narrowing isotropic rotational tumbling[59]. The following analysis refers to data obtained on 0.207 M **I** dissolved in degassed $CDCl_3$ solution acquired at 11.7 T (^{13}C nuclear Larmor frequency = 125.8 MHz) and 25°C. The deuteron quadrupole coupling constant $\omega_Q/2\pi = 96.9$ kHz was estimated by using the quantum chemistry package *Gaussian 09*[68]. NMR computations employed the GIAO-DFT/B3LYP/6-31G+(d,p) level of theory incorporating the use of the keyword "pick-

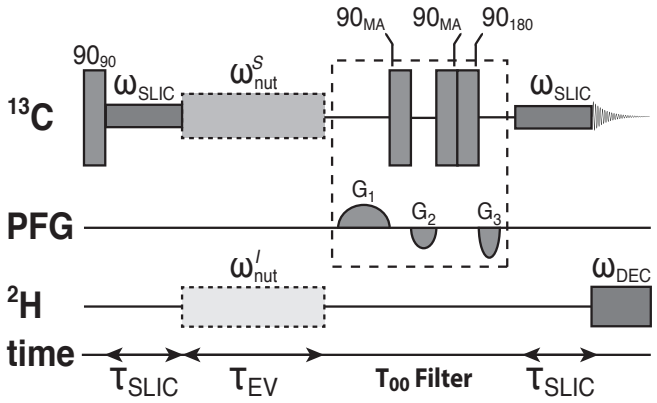

FIG. 15. Pulse sequence for preparing long-lived nuclear singlet order in **I** and monitoring its decay. The experiments used the following parameters: $\omega_{\mathrm{SLIC}}/2\pi = 71.5$ Hz and $\tau_{\mathrm{SLIC}}/2\pi = 27$ ms. The "T_{00} filter" selects out signals that do not pass through nuclear singlet order[36]. "MA" denotes the "magic angle" (54.7°). The grey boxes denote optional "spin-locking" rf fields, with nutation frequencies ω^I_{nut} and ω^S_{nut}, which are active during the singlet evolution delay τ_{EV}. The superscripts I and S denote the ^{2}H and ^{13}C spin-locking rf fields, respectively. An interval of 150 s was used between successive transients.

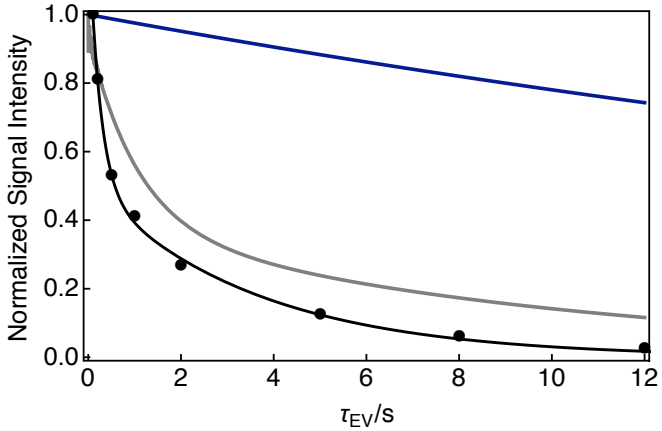

FIG. 16. Experimental relaxation curve (black data points) showing the decay of ^{13}C signal intensity for 0.207 M **I** dissolved in degassed $CDCl_3$ solvent acquired at 11.75 T (^{13}C nuclear Larmor frequency = 125.8 MHz) and 25°C with 2 transients per data point, using the pulse sequence in Figure 15. All experimental signal amplitudes were normalized to the first data point. The decay curve was fitted with a biexponential decay function (black curve): A exp{-t/T_A} + B exp{-t/T_B}. A = 0.772, $T_A = 240 \pm 40$ ms, B = 0.504, $T_B = 3.6 \pm 0.3$ s. A simulated relaxation curve for the decay of ^{13}C nuclear singlet order is shown by the grey curve. The simulation includes dipole-dipole relaxation between the ^{13}C labels and the deuteron sites, ^{13}C CSA relaxation, quadrupolar relaxation for the two deuterons, and the J-coupling network presented in Table I. A simulation neglecting the ^{13}C-^{2}H scalar couplings is shown by the blue curve.

ett"[69]. Default $CDCl_3$ solvent inclusion was chosen. Biaxiality of the quadrupole coupling tensor is small and is neglected. From comparing the experimental relaxation time $T_1(^2\mathrm{H}) = 168 \pm 7$ ms with Equation 55, which was derived for the case of a molecule undergoing isotropic rotational diffusion[48], and assuming that the quadrupolar mechanism dominates the deuteron relaxation, we estimate a correlation time for the overall tumbling of the molecule in solution: $\tau_c = 10.7 \pm 0.5$ ps. The contribution of dipole-dipole interactions to ^{2}H longitudinal relaxation is found to be negligible and is ignored.

A numerical simulation of the the long-lived state decay is shown by the grey curve in Figure 16. The simulation considers a 4-spin system of the $^{13}C_2$ spin pair and the two adjacent deuterons. The deuterons are modelled as spin-1 nuclei.

The numerical simulation propagates the spin density operator (nuclear singlet order) forward in time under the Liouville-von Neumann equation (Equation 3) with a Liouvillian consisting of coherent and incoherent interactions (Equation 4). In this case, the coherent Hamiltonian takes the following form:

$$H_{\mathrm{coh}} = \omega_J S_1 \cdot S_2 + \frac{1}{2}(\omega_\Sigma + \omega_\Delta)(S_{1z} I_{3z} + S_{2z} I_{4z}) + \frac{1}{2}(\omega_\Sigma - \omega_\Delta)(S_{2z} I_{3z} + S_{1z} I_{4z}) + \frac{\Delta\Omega^S_{23}}{2}(S_{2z} - S_{3z}) \tag{57}$$

and includes the complete scalar coupling constant map shown in Figure 13 and the isotropic chemical shift difference between the ^{13}C labelling sites $\Delta\Omega^S_{23} = 2\pi\, 7.75\ \mathrm{rads}^{-1}$ (obtained from the fit of the experimental ^{13}C NMR spectrum of **I**).

The relaxation superoperator has the following composition:

$$\hat{\Gamma} = \hat{\Gamma}^{DD}_S + \hat{\Gamma}^{DD}_{SI} + \hat{\Gamma}^{CSA}_S + \hat{\Gamma}^{Q}_I \tag{58}$$

where $\hat{\Gamma}^{DD}_{SI}$ is the out of pair dipole-dipole relaxation superoperator and $\hat{\Gamma}^{CSA}_S$ is the chemical shift anisotropy (CSA) relaxation superoperator for the ^{13}C spin pair. Cross-correlated relaxation between dipole-dipole, CSA and quadrupolar interactions is included in the simulation.

The following interactions are included in the simulation: (1) the J-coupling network from Table I; (2) quadrupolar relaxation for the deuteron spins, established from the estimates of the deuteron quadrupole coupling constant ω_Q, the rotational correlation time τ_c and Equation 55; (3) ^{13}C-^{2}H dipole-dipole couplings; and (4) CSA for the central ^{13}C nuclei. The relevant parameters and singlet relaxation contributions for the dipole-dipole and CSA interactions are described in the Supplementary Material (SM).

The singlet-triplet leakage relaxation mechanism emerges naturally from the simulation by the virtue of: (*i*) longitudinal relaxation for the *S*-spins; and (*ii*) scalar couplings between the carbon pair and the quadrupolar nuclei. The presence of the out of pair J-couplings and an efficient quadrupolar relaxation mechanism for the coupled spin-1 nuclei introduces the S-SR2K mechanism.

A simulation of the ^{13}C singlet order decay (Figure 16, grey curve) yields a biexponential relaxation curve, which is in respectable agreement with the experimental data, although a discrepancy remains. The discrepancy between experimental and estimated ^{13}C singlet order decay curves could be attributed to additional relaxation mechanisms including: dipole-dipole couplings to remote nuclei in **I** and with molecules in the solvent, and spin-rotation or spin-

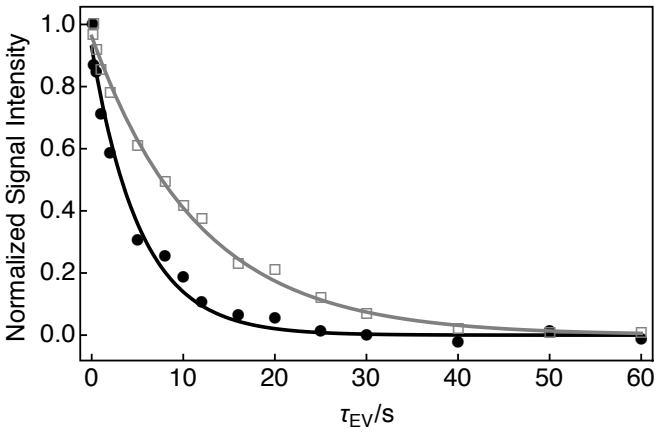

FIG. 17. Experimental relaxation curves showing the decay of ^{13}C nuclear singlet order for 0.207 M **I** dissolved in degassed $CDCl_3$ solvent acquired at 11.75 T (^{13}C nuclear Larmor frequency = 125.8 MHz) and 25°C with 2 transients per data point. The decay of ^{13}C nuclear singlet order was measured by using the pulse sequence described in Figure 15 in the presence of ^{2}H spin-locking rf fields (nutation frequency = $\omega^I_{nut}/2\pi$) during the singlet evolution delay τ_{EV}. Nutation frequencies: Black: $\omega^I_{nut}/2\pi$ = 200 Hz; Grey: $\omega^I_{nut}/2\pi$ = 640 Hz. The singlet relaxation time constants are: Black filled circles: T_S = 5.3 ± 0.4 s; Grey open squares: T_S = 11.7 ± 0.4 s. All the fitted curves have a single exponential form. All signal amplitudes were normalized to the first data point.

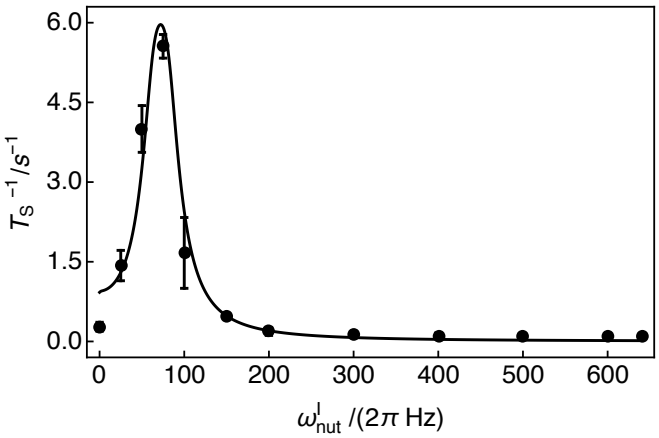

FIG. 18. Black data points: experimental dependence of the singlet lifetime T_S^{-1} on ^{2}H spin-locking rf field amplitudes (nutation frequency = $\omega^I_{nut}/2\pi$) for 0.207 M **I** dissolved in degassed $CDCl_3$ solvent acquired at 11.75 T (^{13}C nuclear Larmor frequency = 125.8 MHz) and 25°C. Black curve: simulated dependence of T_S^{-1} on $\omega^I_{nut}/2\pi$. Simulations include singlet relaxation from the SR2K mechanism only.

internal-motion couplings[33,39,70].

The good match of the simulation to the experimental data, including the prominent biexponentiality of the decay, strongly supports the hypothesis that the relaxation of nuclei which have J-couplings to the $^{13}C_2$ spin pair induce singlet relaxation by a S-SR2K mechanism.

The importance of the S-SR2K mechanism may be tested by considering a second simulation (blue curve) in which the quadrupolar relaxation of the two deuterons is disconnected to the constituent nuclei of the singlet state by setting the ^{13}C-^{2}H scalar couplings to zero, while leaving all other interactions unchanged. In this case, the simulation returns a much slower monoexponential decay (blue curve) which is clearly inconsistent with the experimental data. We conclude that scalar-relaxation-of-the-second-kind is a dominant relaxation mechanism for $^{13}C_2$ singlet order in this system.

B. Application of a ^{2}H rf field

Experimental relaxation curves showing the decay of ^{13}C nuclear singlet order for **I** in the presence of on resonant ^{2}H spin-locking rf fields are presented in Figure 17.

The black curve in Figure 17 shows the decay of ^{13}C nuclear singlet order with coherent continuous wave irradiation, $\omega^I_{nut}/2\pi$ = 200 Hz nutation frequency, applied to the ^{2}H spins. The decay is monoexponential and has a decay time constant: T_S = 5.3 ± 0.4 s. The grey curve in Figure 17 displays the decay of ^{13}C nuclear singlet order in the presence of ^{2}H CW irradiation with $\omega^I_{nut}/2\pi$ = 640 Hz nutation frequency. The singlet relaxation time constant is T_S = 11.7 ± 0.4 s. In agreement with the theory presented in section II D, the application of a resonant rf field on the ^{2}H nuclei (*I*-spins) suppresses the singlet-SR2K mechanism and extends the singlet lifetime T_S.

The experimental singlet relaxation rate constants T_S^{-1} as a function of ^{2}H spin-locking rf field amplitude, expressed as the nutation frequency $\omega^I_{nut}/2\pi$, are shown by the black data points in Figure 18. Numerically determined singlet relaxation rate constants are shown by the black curve. Simulations include singlet relaxation from the SR2K mechanism only.

The experimental singlet relaxation rate constants T_S^{-1} increase dramatically, and reach a maximum, as $\omega^I_{nut}/2\pi$ approaches J_{23} = 71.5 Hz, corresponding to a match between the ^{2}H nutation frequency and the ^{13}C-^{13}C J-coupling, as predicted by the theory given above. The experimental and numerical curves are in excellent agreement. The experimental singlet relaxation rate constants T_S^{-1} decrease with increasing ^{2}H spin-locking rf field amplitude, beyond a nutation frequency of ∼150 Hz. The ^{13}C singlet relaxation time constant at the largest ^{2}H nutation frequency of $\omega^I_{nut}/2\pi = 640$ Hz is given by $T_S = 11.7 \pm 0.4$ s, corresponding to a rate constant of $T_S^{-1} = (85 \pm 3) \times 10^{-3}$ s^{-1}. Further increases in ^{2}H rf field amplitudes were precluded by instrumental limitations. Although the application of a strong ^{2}H rf field greatly extended the lifetime of the ^{13}C singlet state, the longest observed time constant T_S was still shorter than the spin-lattice relaxation time constant $T_1(^{13}C) = 14.0 \pm 0.5$ s in the same system.

The singlet relaxation rate constant T_S^{-1} can be predicted in the presence of an on resonant radiofrequency field applied continuously to the deuterium nuclei throughout the singlet evolution interval τ_{EV}. By using Equation 43, which applies for extreme-narrowing isotropic rotational tumbling, the estimate of the longitudinal relaxation time for the ^{2}H nucleus (which was consequently used for the estimate of the rota-

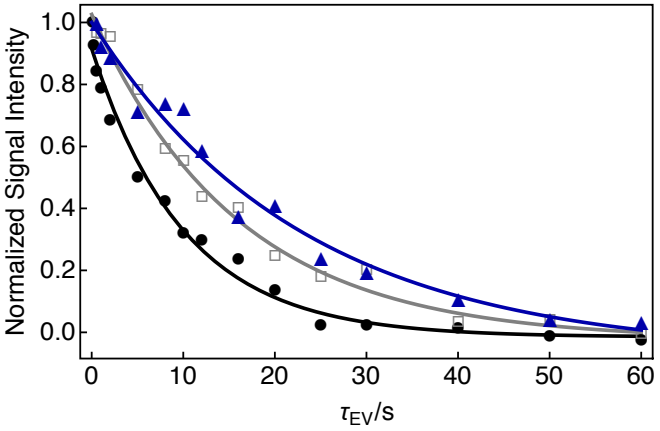

FIG. 19. Experimental relaxation curves showing the decay of ^{13}C nuclear singlet order for 0.207 M **I** dissolved in degassed $CDCl_3$ solvent acquired at 11.75 T (^{13}C nuclear Larmor frequency = 125.8 MHz) and 25°C with 2 transients per data point. The decay of ^{13}C nuclear singlet order was measured by using the pulse sequence in Figure 15 in the presence of ^{13}C spin-locking rf fields (nutation frequency = $\omega^S_{nut}/2\pi$) during the singlet evolution delay τ_{EV}. Nutation frequencies: Black: $\omega^S_{nut}/2\pi$ = 200 Hz; Grey: $\omega^S_{nut}/2\pi$ = 600 Hz; Blue: $\omega^S_{nut}/2\pi$ = 1 kHz. The singlet relaxation time constants are: Black filled circles: T_S = 9.6 ± 0.6 s; Grey open squares: T_S = 16 ± 1 s; Blue filled triangles: T_S = 23 ± 4 s. All the fitted curves have a single exponential form. All signal amplitudes were normalized to the first data point.

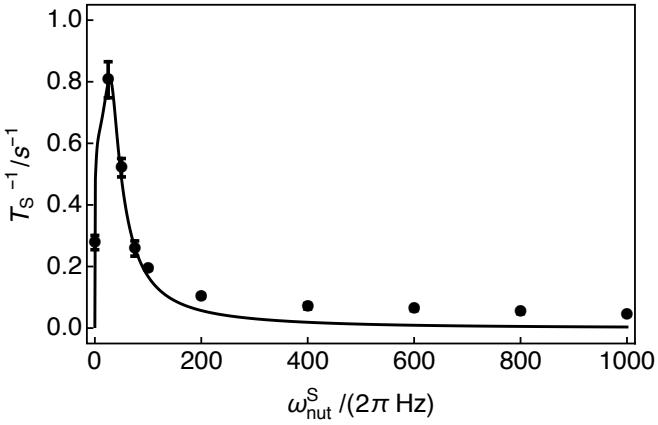

FIG. 20. Black data points: experimental dependence of the singlet lifetime T_S^{-1} on ^{13}C spin-locking rf field amplitudes (nutation frequency = $\omega^S_{nut}/2\pi$) for 0.207 M **I** dissolved in degassed $CDCl_3$ solvent acquired at 11.75 T (^{13}C nuclear Larmor frequency = 125.8 MHz) and 25°C. The first data point corresponds to $\omega^S_{nut}/2\pi$ = 0 Hz. Black curve: simulated dependence of T_S^{-1} on $\omega^S_{nut}/2\pi$. Simulations include singlet relaxation from the SR2K mechanism only.

tional correlation time τ_c), the in pair ^{13}C-^{13}C dipole-dipole coupling constant (see the Supplementary Material (SM)), and the spin system parameters obtained from fitting the experimental ^{13}C NMR spectrum, the following prediction of the singlet relaxation rate constant in the presence of CW irradiation resonant with the deuterium spins with 640 Hz nutation frequency is obtained: $T_S^{-1}(\omega^I_{nut}/2\pi = 640\,\text{Hz}) = (6.4 \pm 0.5) \times 10^{-3}\,\text{s}^{-1}$. As shown in the Supplementary Material (SM), dipole-dipole couplings from the central ^{13}C nuclei to the adjacent deuteron spins are expected to provide an additional contribution to the singlet relaxation rate constant: $T_S^{-1}(\text{DD}) = (25 \pm 1) \times 10^{-3}\,\text{s}^{-1}$. These combined mechanisms predict a value of T_S of 31.8 ± 0.9 s, which is considerably longer than that found experimentally. The discrepancy is provisionally attributed to other relaxation mechanisms such as: long-range intramolecular dipole-dipole couplings, intermolecular dipole-dipole couplings, paramagnetic relaxation associated with molecular oxygen dissolved in solution, and spin-rotation or spin-internal-motion[33,39,70]. We have not investigated these issues further.

C. Application of a ^{13}C rf field

Experimental relaxation curves showing the decay of ^{13}C nuclear singlet order for **I** in the presence of on resonant ^{13}C rf fields are presented in Figure 19.

The decays have a single exponential form in all cases, with the singlet decay time constant increasing from $T_S = 9.6 \pm 0.6$ s for a ^{13}C field with nutation frequency of 200 Hz, to a time constant of $T_S = 23 \pm 4$ s with a ^{13}C nutation frequency of 1 kHz. Further increases in ^{13}C rf field amplitudes were precluded by instrumental limitations. Note that the singlet lifetime of 23 s exceeds the ^{13}C spin-lattice relaxation time constant of $T_1(^{13}\text{C}) = 14.0 \pm 0.5$ s in the same system.

The experimental singlet relaxation rate constants T_S^{-1} as a function of ^{13}C spin-locking rf field amplitude, expressed as the nutation frequency $\omega^S_{nut}/2\pi$, are shown by the black data points in Figure 20. The first data point corresponds to $\omega^S_{nut}/2\pi = 0$ Hz. Numerically determined singlet relaxation rate constants are shown by the black curve. Simulations include singlet relaxation from the SR2K mechanism only.

The numerical simulation shows dramatic increase in the singlet relaxation rate constants T_S^{-1} with the application of only a weak rf field on the *S*-spins, in agreement with the simulations presented in section II D. A maximum experimental singlet relaxation rate constant is observed at approximately $\omega^S_{nut}/2\pi$ = 25 Hz, in agreement with the numerical simulation. The profile of the experimental and numerical curves are in good agreement.

The singlet decay rate constants T_S^{-1} decrease with increasing ^{13}C rf field amplitude beyond a nutation frequency of $\omega^S_{nut}/2\pi \sim 100$ Hz. A discrepancy between experimental and numerical results is observed in this case, and is attributed to additional relaxation mechanisms, such as the ^{13}C-^{2}H dipole-dipole contribution.

D. Simultaneous rf fields on ^{2}H and ^{13}C nuclei

A further extension in ^{13}C singlet lifetime is achieved by applying simultaneous rf fields resonant with the ^{13}C and ^{2}H nuclei (see Figure 21). In this case, the two fields have a cumulative effect on the suppression of the singlet-scalar relax-

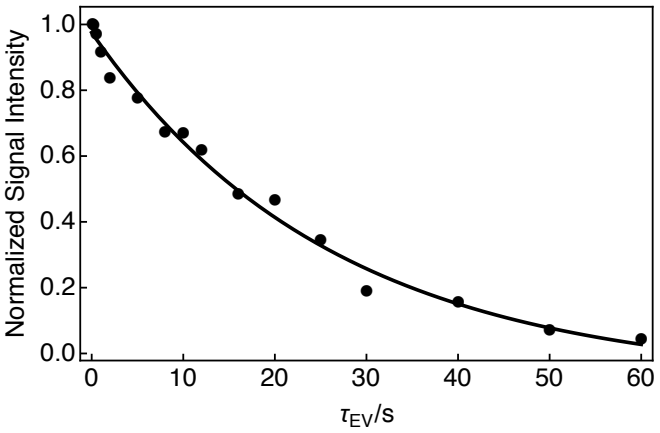

FIG. 21. Experimental relaxation curve showing the decay of ^{13}C nuclear singlet order for 0.207 M **I** dissolved in degassed $CDCl_3$ solvent acquired at 11.75 T (^{13}C nuclear Larmor frequency = 125.8 MHz) and 25°C with 2 transients per data point. The decay of ^{13}C nuclear singlet order was measured by using the pulse sequence described in Figure 15 in the presence of simultaneous ^{2}H and ^{13}C rf fields, with nutation frequencies $\omega^I_{\rm nut} = 640$ Hz and $\omega^S_{\rm nut} = 1$ kHz, respectively, during the singlet evolution delay $\tau_{\rm EV}$. The singlet relaxation time constant is: $T_{\rm S} = 26 \pm 3$ s. The fitted curve has a single exponential form. All signal amplitudes were normalized to the first data point.

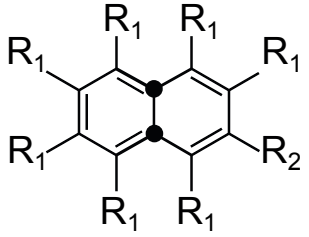

FIG. 22. Molecular structure of the $^{13}C_2$-naphthalene derivative here denoted **II**[33]. Black circles denote ^{13}C nuclei. $R^1 = OCD_3$, $R^2 = OCD(CD_3)_2$. The $^{13}C_2$-naphthalene derivative has 28 remote deuterons.

ation mechanism. Simultaneous rf fields with a nutation frequency of $\omega^I_{\rm nut}/2\pi = 640$ Hz for ^{2}H, and $\omega^S_{\rm nut}/2\pi = 1$ kHz for ^{13}C, achieved a singlet decay time constant of $T_{\rm S} = 26 \pm 3$ s. This is almost twice as long as the ^{13}C T_1 for the same system.

V. DISCUSSION

The theoretical analysis and experimental results shown above confirm that the scalar-relaxation-of-the-second-kind (SR2K) mechanism may be an important mechanism of nuclear singlet relaxation. The mechanism requires that the relevant spin pair has significant J-couplings with nuclei which themselves relax moderately rapidly. In particular, deuterium nuclei often relax with appropriate rate constants, and are likely to be significant contributors to the SR2K mechanism of nuclear singlet relaxation.

Unlike purely incoherent relaxation mechanisms, such as the dipole-dipole mechanism, the SR2K mechanism involves a combination of coherent and incoherent terms, and may be effectively suppressed by the application of resonant rf fields.

It is interesting to speculate whether the SR2K mechanism could contribute significantly to singlet relaxation phenomena which have already appeared in the literature. Examples include those in references[26–28,33–35].

Consider, for example, the case of the $^{13}C_2$-labelled naphthalene derivative studied in reference[33] and here denoted **II** (see Figure 22). This compound displays an exceptionally long ^{13}C singlet lifetime, which exceeds $T_{\rm S} = 1$ hour for a degassed solution in low magnetic field[33]. Could this long lifetime be limited by weak SR2K effects from the 28 remote deuterons?

The ^{2}H T_1 has been estimated to be $(905 \pm 45) \times 10^{-3}$ s by an inversion-recovery experiment for **II** dissolved in degassed acetone-d_6 solvent acquired at 9.4 T (nuclear Larmor frequency = 61.4 MHz) and 25°C. The measured ^{2}H longitudinal relaxation time is relatively long compared to typical deuteron relaxation times in solution, presumably reflecting the high mobility of the deuterated side chains.

The contribution of SR2K relaxation to the singlet lifetime of **II** is estimated by analysing the deuteron relaxation time $T_1(^2{\rm H}) = (905 \pm 45) \times 10^{-3}\,{\rm s}^{-1}$ using Equation 37.

For simplicity, assume that the differential J-coupling ω_Δ is the same for all 28 deuterons. The total contribution to the ^{13}C singlet relaxation rate constant is given approximately by:

$$T_{\rm S}^{-1}({\rm from}\,^2{\rm H}) \simeq 28 \times {\rm eqn}\,37 \tag{59}$$

$$\simeq 43.8 \times 10^{-6}\ {\rm s} \times \omega_\Delta^2 \tag{60}$$

using $R_1^S = (3/2)\, b_{\rm CC}^2 \tau_c$ and the following spin system parameters: $\omega_J/2\pi = 54.6$ Hz, $\tau_c = 20$ ps, and $b_{\rm CC}/2\pi = -2.654$ kHz (estimated from a ^{13}C-^{13}C internuclear separation of 142 pm).

Equation 59 is a strong function of the differential J-coupling ω_Δ. It is hard to obtain an experimental estimate of this parameter, since the ^{2}H-^{13}C couplings are too small to resolve. Quantum chemistry calculations may be feasible but would have to take into account the conformational flexibility and have not been attempted at this stage.

Nevertheless we note that the observed $^{13}C_2$ singlet relaxation rate constant of $0.21 \pm 0.02\ 10^{-3}\ {\rm s}^{-1}$[33] could be fully attributed to the SR2K mechanism if all 28 remote deuterons had a differential coupling of only $|\omega_\Delta/2\pi| = 0.35$ Hz to the two ^{13}C nuclei. This value is not wildly unreasonable. The issue could be settled by applying resonant ^{2}H or ^{13}C irradiation in an attempt to further extend the ^{13}C singlet relaxation time by suppressing the SR2K mechanism. The resonant irradiation would have to be applied in low magnetic field. This experiment is planned.

VI. CONCLUSION

We conclude that the SR2K mechanism may be an important contribution to limiting long singlet lifetimes, and cannot

be neglected, even in the case of remote quadrupolar spins.

It should be noted that other interesting molecules may also exhibit S-SR2K. Systems comprising of H_2C=CD-CO_2R substructures, such as styrene-d_1, are of suitable type. However, the S-SR2K mechanism may only be isolated through implementing field cycling experiments as the large proton chemical shift difference introduces relaxation contributions from singlet-triplet leakage. It is also not yet known whether the proton singlet state of H_2C=CX-CO_2R systems, where X is a quadrupolar nucleus relaxing on the timescale of the proton nuclear Larmor frequency, such as Br or Cl, display observable S-SR2K. Investigations into this effect are feasible on molecular systems such as bromoacrylates and bromothiophenes but would require detailed computational modelling or molecular dynamics, and also measurement of the quadrupolar X-atom T_1.

SUPPLEMENTARY MATERIAL

See supplementary material for details regarding chemical synthesis, experimental methods, quantum chemistry, and numerical simulations.

ACKNOWLEDGMENTS

This work was supported by the Engineering and Physical Sciences Research Council (EPSRC) UK, grant codes EP/P009980/1, EP/N002482/1 and EP/L505067/1, Bruker Biospin UK and the Wolfson Foundation. The authors gratefully acknowledge Ilya Kuprov (University of Southampton) for assistance with *Spinach* simulations, and Gabriele Stevanato (EPFL) for enlightening discussions.

APPENDIX: PERTURBATIVE TREATMENT

A. Effective Hamiltonian via Primas-van Vleck perturbation theory

Consider the standard perturbation problem where the eigenstates and eigenvalues of the main Hamiltonian, H_0, are perturbed by λV with $\lambda \ll 1$:

$$H = H_0 + \lambda V. \tag{61}$$

In most cases, an approximate solution may be derived by Rayleigh-Schrödinger perturbation theory[71]. In the case of degenerate or near-degenerate eigenvalues, the Rayleigh-Schrödinger approach becomes difficult. For the current problem, we prefer the Primas-van-Vleck perturbation approach, also called the contact transformation, rather than the Rayleigh-Schrödinger approach[61–65].

The set of eigenvalues of H_0 is called the spectrum of H_0 and is denoted by:

$$\begin{gathered}\sigma(H_0) = \{\lambda_1, \lambda_2, \ldots, \lambda_N\} \\ H_0|n_j\rangle = \lambda_1|n_j\rangle.\end{gathered} \tag{62}$$

A particular eigenvalue of H_0 may be degenerate so that more than one eigenvector may belong to the same eigenvalue. We denote the multiplicity of an eigenvalue by D_j and distinguish the corresponding eigenvectors by introducing a second label $|n_{jk}\rangle$. The degenerate eigenvectors fulfill the equation:

$$H_0\left(\sum_{k=1}^{D_j} c_{jk}|n_{jk}\rangle\right) = \lambda_j\left(\sum_{k=1}^{D_j} c_{jk}|n_{jk}\rangle\right) \tag{63}$$

and span a D_j dimensional eigenspace of λ_j. The projection superoperator onto the eigenspace belonging to the eigenvalue λ_j is defined as:

$$\begin{aligned}\hat{P}_j &= \sum_{k=1}^{D_j} |n_{jk}\rangle\langle n_{jk}| \bullet |n_{jk}\rangle\langle n_{jk}| \\ \hat{P}_j Q &= \sum_{k=1}^{D_j} |n_{jk}\rangle\langle n_{jk}|Q|n_{jk}\rangle\langle n_{jk}|.\end{aligned} \tag{64}$$

Consider the sum of all such projection superoperators:

$$\hat{P}_0 = \sum_{j=1}^{N} \hat{P}_j. \tag{65}$$

The superoperator $\hat{P}_0$ may be used to decompose any operator into a parallel (commuting) and anti-parallel (non-commuting) part with respect to H_0:

$$\begin{gathered}Q_\parallel = \hat{P}_0 Q \quad Q_\perp = \mathbb{1} - Q_\parallel \\ \hat{P}_0 Q_\parallel = Q_\parallel \quad \hat{P}_0 Q_\perp = 0.\end{gathered} \tag{66}$$

Parallel and anti-parallel parts remain parallel and anti-parallel upon commutation with H_0:

$$= 0 \quad [H_0, Q_\perp] = S_\perp \tag{67}$$

with $S_\perp$ being some anti-parallel operator.

With these considerations in place we slightly reformulate the perturbation problem. We are searching for a unitary transformation superoperator $\hat{U}$ that block-diagonalizes H. In general the action of the superoperator $\hat{U}$ may be expressed as shown below:

$$\begin{aligned}\hat{U}H &= H_0 + W \\ W &= \hat{U}H - H_0.\end{aligned} \tag{68}$$

Here W is a block-diagonal operator, still to be determined. This approach amounts to removing off-diagonal elements between different eigenspaces of H_0. The transformation superoperator $\hat{U}$ is generally given by the exponential of an anti-hermitian generator $\hat{G}$:

$$\hat{U} = \exp(\hat{G}) \quad \hat{G}^\dagger = -\hat{G}. \tag{69}$$

The choice of $\hat{G}$ is ill-defined at this point since any unitary equivalent form of $\hat{G}$ would lead to an unitary equivalent representation. This issue is circumvented by imposing the following constraints:

$$\hat{P}_0 G = 0 \quad \hat{P}_0 W = W. \tag{70}$$

A perturbative solution to equation 68 is constructed by expanding $\hat{G}$ and W in powers of λ:

$$\begin{aligned}\hat{G} &= \lambda\hat{G}_1 + \lambda^2\hat{G}_2 + \dots \\ W &= \lambda W_1 + \lambda^2 W_2 + \dots\end{aligned} \tag{71}$$

Truncating W at a certain point leads to an effective Hamiltonian within the eigenspaces of H_0. Substitution of the power series expansion into equation 68 leads to:

$$\begin{aligned}\lambda W_1 + \lambda^2 W_2 + \dots &= \left(\sum_{n=0}^{\infty}\frac{1}{n!}\hat{G}^n H\right) - H_0 \\ &= \lambda V \\ &\quad + (\lambda\hat{G}_1 + \lambda^2\hat{G}_2 + \dots)H \\ &\quad + (\lambda\hat{G}_1 + \lambda^2\hat{G}_2 + \dots)^2 H \\ &\quad + \dots\end{aligned} \tag{72}$$

Collecting terms of the same power in λ leads to recursive commutator equations of the type:

$$\begin{aligned}\hat{H}_0 G_1 &= V - W_1 = A_1 - W_1 \\ \hat{H}_0 G_2 &= \hat{G}_1 V + \frac{1}{2}\hat{G}_1^2 H_0 - W_2 = A_2 - W_2 \\ &\dots \\ \hat{H}_0 G_n &= A_n - W_n.\end{aligned} \tag{73}$$

We may solve for W_n by making use of the properties in equation 67 and the constraints of equation 70:

$$\begin{aligned}\hat{P}_0(\hat{H}_0 G_n) = 0 \quad \hat{P}_0 A_n - \hat{P}_0 W_n &= \hat{P}_0 A_n - W_n \\ \implies W_n &= \hat{P}_0 A_n.\end{aligned} \tag{74}$$

The result for W_n may then be substituted back into equation 73. To solve for G_n we calculate the pseudo-inverse of $\hat{H}_0$. The solution to the perturbative treatment is therefore given by:

$$\begin{aligned}W_n &= \hat{P}_0 A_n \\ G_n &= \hat{H}_0^+(A_n - W_n) = \hat{H}_0^+(A_n - \hat{P}_0 A_n).\end{aligned} \tag{75}$$

B. Application of Primas-van Vleck perturbation theory

We applied Primas-van Vleck perturbation theory in section 2.3 to derive the analytic expressions for the various spin-lock cases. We illustrate the method for the simplest case of no applied rf fields. The other results may be obtained in a similar manner.

As explained in the main text, the dynamics of this case may be restricted to a 4×4 block of the full Liouvillian. The relevant block takes the form:

$$\begin{pmatrix} 0 & 0 & 0 & -i\omega_\Delta/\sqrt{6} \\ 0 & -\frac{3}{5}R_1^S & 0 & i\omega_\Delta/2\sqrt{6} \\ 0 & 0 & -R_1^I - \frac{1}{3}R_1^S & -i\omega_J \\ -i\omega_\Delta/\sqrt{6} & i\omega_\Delta/2\sqrt{6} & -i\omega_J & -R_1^I - \frac{1}{3}R_1^S \end{pmatrix}. \tag{76}$$

We attempt to find a perturbative solution by making the following assumption:

$$\begin{aligned}L_0 + L_1 = &\begin{pmatrix} 0 & 0 & 0 & 0 \\ 0 & -\frac{3}{5}R_1^S & 0 & 0 \\ 0 & 0 & -R_1^I - \frac{1}{3}R_1^S & -i\omega_J \\ 0 & 0 & -i\omega_J & -R_1^I - \frac{1}{3}R_1^S \end{pmatrix} \\ &+ \begin{pmatrix} 0 & 0 & 0 & -i\omega_\Delta/\sqrt{6} \\ 0 & 0 & 0 & i\omega_\Delta/2\sqrt{6} \\ 0 & 0 & 0 & 0 \\ -i\omega_\Delta/\sqrt{6} & i\omega_\Delta/2\sqrt{6} & 0 & 0 \end{pmatrix}.\end{aligned} \tag{77}$$

To get reasonable results it is important to notice that the separation between the eigenvalues 0 and $-\frac{3}{5}R_1^S$ is not big enough to ignore the state mixing of $|1\rangle$ and $|2\rangle$. As a result the set $\{|1\rangle, |2\rangle\}$ forms a quasi-degenerate manifold and the set $\{|3\rangle, |4\rangle\}$ forms a degenerate manifold. The projector $\hat{P}_0$ onto the subspace of L_0 is consequently given by:

$$\begin{aligned}\hat{P}_0 Q = &(|1\rangle\langle 1| + |2\rangle\langle 2|)Q(|1\rangle\langle 1| + |2\rangle\langle 2|) \\ &+ (|3\rangle\langle 3| + |4\rangle\langle 4|)Q(|3\rangle\langle 3| + |4\rangle\langle 4|).\end{aligned} \tag{78}$$

Equation 73 shows that the anti-hermitian generator, $\hat{G}$, of the transformation is recursively determined from H_0 and V. For problems in Hilbert space H and V will be hermitian. For generators in Liouville space such as L_0 and L_1 this might not be true in general. For the current cases we may choose L_0 and L_1 to be hermitian, so that Primas-van Vleck perturbation theory remains valid. The effective Liouvillian to second order may then be written as:

$$L_{eff} = L_0 + \lambda\hat{P}_0 A_1 + \lambda^2\hat{P}_0 A_2. \tag{79}$$

The first order term is given by:

$$\begin{aligned}W_1 = &\begin{pmatrix} 1 & 0 & 0 & 0 \\ 0 & 1 & 0 & 0 \\ 0 & 0 & 0 & 0 \\ 0 & 0 & 0 & 0 \end{pmatrix} \begin{pmatrix} 0 & 0 & 0 & -i\omega_\Delta/\sqrt{6} \\ 0 & 0 & 0 & i\omega_\Delta/2\sqrt{6} \\ 0 & 0 & 0 & 0 \\ -i\omega_\Delta/\sqrt{6} & i\omega_\Delta/2\sqrt{6} & 0 & 0 \end{pmatrix} \begin{pmatrix} 1 & 0 & 0 & 0 \\ 0 & 1 & 0 & 0 \\ 0 & 0 & 0 & 0 \\ 0 & 0 & 0 & 0 \end{pmatrix} \\ &+ \begin{pmatrix} 0 & 0 & 0 & 0 \\ 0 & 0 & 0 & 0 \\ 0 & 0 & 1 & 0 \\ 0 & 0 & 0 & 1 \end{pmatrix} \begin{pmatrix} 0 & 0 & 0 & -i\omega_\Delta/\sqrt{6} \\ 0 & 0 & 0 & i\omega_\Delta/2\sqrt{6} \\ 0 & 0 & 0 & 0 \\ -i\omega_\Delta/\sqrt{6} & i\omega_\Delta/2\sqrt{6} & 0 & 0 \end{pmatrix} \begin{pmatrix} 0 & 0 & 0 & 0 \\ 0 & 0 & 0 & 0 \\ 0 & 0 & 1 & 0 \\ 0 & 0 & 0 & 1 \end{pmatrix} \\ = &\begin{pmatrix} 0 & 0 & 0 & 0 \\ 0 & 0 & 0 & 0 \\ 0 & 0 & 0 & 0 \\ 0 & 0 & 0 & 0 \end{pmatrix}.\end{aligned} \tag{80}$$

As a result the recursion for the generator to first order may be evaluated to give:

$$G_1 = \begin{pmatrix} 0 & 0 & -3\sqrt{\frac{3}{2}}\frac{\omega_J}{(3R_1^I+R_1^S)^2} \\ 0 & 0 & \frac{75}{2}\sqrt{3}\frac{\omega_J}{(15R_1^I-4R_1^S)^2} \\ 3\sqrt{\frac{3}{2}}\frac{\omega_J}{(3R_1^I+R_1^S)^2+9\omega_J^2} & -\frac{75}{2}\sqrt{3}\frac{\omega_J}{(15R_1^I-4R_1^S)^2+225\omega_J^2} & 0 \\ -i\sqrt{\frac{3}{2}}\frac{(3R_1^I+R_1^S)}{(3R_1^I+R_1^S)^2+9\omega_J^2} & -i5\sqrt{3}\frac{(15R_1^I-4R_1^S)}{2(15R_1^I-4R_1^S)^2+450\omega_J^2} & 0 \end{pmatrix} \tag{81}$$

Such that the second order correction amounts to:

$$W_2 = \begin{pmatrix} -\frac{3R_1^I+R_1^S}{2((3R_1^I+R_1^S)^2+9\omega_J^2)} & \frac{1}{4\sqrt{2}}\frac{(30+R_1^I+R_1^S)((15R_1^I-4R_1^S)(3R_1^I+R_1^S)+45\omega_J)}{((3R_1^I+R_1^S)+9\omega_J^2((15R_1^I-4R_1^S)225\omega_J^2))} \\ \frac{1}{4\sqrt{2}}\frac{(30+R_1^I+R_1^S)((15R_1^I-4R_1^S)(3R_1^I+R_1^S)+45\omega_J)}{((3R_1^I+R_1^S)+9\omega_J^2((15R_1^I-4R_1^S)225\omega_J^2))} & -\frac{75R_1^I-20R_1^S}{4(15R_1^I-4R_1^S)^2+900\omega_J^2} \end{pmatrix} \bigoplus \begin{pmatrix} 0 & -i\,\frac{9}{8}\frac{\omega_J(225{R_1^I}^2-30R_1^IR_1^S+19{R_1^S}^2+225\omega_J^2)}{((3R_1^I+R_1^S)^2+9\omega_J^2)((15R_1^I-4R_1^S)^2+225\omega_J^2)} \\ -i\,\frac{9}{8}\frac{\omega_J(225{R_1^I}^2-30R_1^IR_1^S+19{R_1^S}^2+225\omega_J^2)}{((3R_1^I+R_1^S)^2+9\omega_J^2)((15R_1^I-4R_1^S)^2+225\omega_J^2)} & \frac{3R_1^I+R_1^S}{2((3R_1^I+R_1^S)^2+9\omega_J)}+\frac{75R_1^I-20R_1^S}{4(15R_1^I-4R_1^S)^2+900\omega_J^2} \end{pmatrix} \tag{82}$$

The general structure of the effective Liouvillian is given by:

$$L_{eff} = \begin{pmatrix} \square & \square & 0 & 0 \\ \square & \square & 0 & 0 \\ 0 & 0 & \square & \square \\ 0 & 0 & \square & \square \end{pmatrix}. \tag{83}$$

The decay rate R_{LLS} may be obtained by solving the quadratic equation in the upper 2×2 block and the result is given in Equation 37 of the main text. The decay rate constants under spin-locking were derived in similar fashion where special care has been taken to identify quasi-degenerate states.

[1] M. Carravetta, O. G. Johannessen and M. H. Levitt, *Phys. Rev. Lett.*, 2004, **92**, 153003.
[2] M. Carravetta and M. H. Levitt, *J. Am. Chem. Soc.*, 2004, **126**, 6228–6229.
[3] M. Carravetta and M. H. Levitt, *J. Chem. Phys.*, 2005, **122**, 214505.
[4] G. Pileio and M. H. Levitt, *J. Magn. Reson.*, 2007, **187**, 141–145.
[5] A. K. Grant and E. Vinogradov, *J. Magn. Reson.*, 2008, **193**, 177–190.
[6] G. Pileio, M. Carravetta, E. Hughes and M. H. Levitt, *J. Am. Chem. Soc.*, 2008, **130**, 12582–12583.
[7] G. Pileio and M. H. Levitt, *J. Chem. Phys.*, 2009, **130**, 214501.
[8] P. R. Vasos, A. Comment, R. Sarkar, P. Ahuja, S. Jannin, J.-P. Ansermet, J. A. Konter, P. Hautle, B. van den Brandt and G. Bodenhausen, *Proc. Natl. Acad. Sci. U.S.A.*, 2009, **106**, 18469–18473.
[9] W. S. Warren, E. Jenista, R. T. Branca and X. Chen, *Science*, 2009, **323**, 1711–1714.
[10] G. Pileio, M. Carravetta and M. H. Levitt, *Proc. Natl. Acad. Sci. U.S.A.*, 2010, **107**, 17135–17139.
[11] M. C. D. Tayler, S. Marie, A. Ganesan and M. H. Levitt, *J. Am. Chem. Soc.*, 2010, **132**, 8225–8227.
[12] G. Pileio, *J. Chem. Phys.*, 2011, **134**, 214505.
[13] M. C. D. Tayler and M. H. Levitt, *Phys. Chem. Chem. Phys.*, 2011, **13**, 5556–5560.
[14] Y. Feng, R. M. Davis and W. S. Warren, *Nat. Phys.*, 2012, **8**, 831–837.
[15] M. B. Franzoni, L. Buljubasich, H. W. Spiess and K. Münnemann, *J. Am. Chem. Soc.*, 2012, **134**, 10393–10396.
[16] G. Pileio, J. T. Hill-Cousins, S. Mitchell, I. Kuprov, L. J. Brown, R. C. D. Brown and M. H. Levitt, *J. Am. Chem. Soc.*, 2012, **134**, 17494–17497.
[17] M. H. Levitt, *Annu. Rev. Phys. Chem.*, 2012, **63**, 89–105.
[18] S. J. DeVience, R. L. Walsworth and M. S. Rosen, *Phys. Rev. Lett.*, 2013, **111**, 173002.
[19] M. C. D. Tayler, I. Marco-Rius, M. I. Kettunen, K. M. Brindle, M. H. Levitt and G. Pileio, *J. Am. Chem. Soc.*, 2012, **134**, 7668–7671.
[20] G. Pileio, S. Bowen, C. Laustsen, M. C. D. Tayler, J. T. Hill-Cousins, L. J. Brown, R. C. D. Brown, J.-H. Ardenkjaer-Larsen and M. H. Levitt, *J. Am. Chem. Soc.*, 2013, **135**, 5084–5088.
[21] Y. Feng, T. Theis, X. Liang, Q. Wang, P. Zhou and W. S. Warren, *J. Am. Chem. Soc.*, 2013, **135**, 9632–9635.
[22] T. Theis, Y. Feng, T. Wu and W. S. Warren, *J. Chem. Phys.*, 2014, **140**, 014201.
[23] Y. Zhang, P. C. Soon, A. Jerschow and J. W. Canary, *Angew. Chem. Int. Ed.*, 2014, **53**, 3396–3399.
[24] A. Bornet, X. Ji, D. Mammoli, B. Vuichoud, J. Milani, G. Bodenhausen and S. Jannin, *Chem. – A Eur. J.*, 2014, **20**, 17113–17118.
[25] K. Claytor, T. Theis, Y. Feng and W. S. Warren, *J. Magn. Reson.*, 2014, **239**, 81–86.
[26] K. Claytor, T. Theis, Y. Feng, J. Yu, D. Gooden and W. S. Warren, *J. Am. Chem. Soc.*, 2014, **136**, 15118–15121.
[27] J.-N. Dumez, J. T. Hill-Cousins, R. C. D. Brown and G. Pileio, *J. Magn. Reson.*, 2014, **240**, 27–30.
[28] G. Pileio, J.-N. Dumez, I. A. Pop, J. T. Hill-Cousins and R. C. D. Brown, *J. Magn. Reson.*, 2015, **252**, 130–134.
[29] D. Mammoli, B. Vuichoud, A. Bornet, J. Milani, J.-N. Dumez, S. Jannin and G. Bodenhausen, *J. Phys. Chem. B*, 2015, **119**, 4048–4052.
[30] A. S. Kiryutin, H. Zimmermann, A. V. Yurkovskaya, H.-M. Vieth and K. L. Ivanov, *J. Magn. Reson.*, 2015, **261**, 64–72.
[31] Y. Zhang, K. L. Bassfeld, J. W. Canary and A. Jerschow, *Phys. Chem. Chem. Phys.*, 2015, **17**, 24370–24375.
[32] G. Stevanato, S. Singha Roy, J. Hill-Cousins, I. Kuprov, L. J. Brown, R. C. D. Brown, G. Pileio and M. H. Levitt, *Phys. Chem. Chem. Phys.*, 2015, **17**, 5913–5922.
[33] G. Stevanato, J. T. Hill-Cousins, P. Håkansson, S. S. Roy, L. J. Brown, R. C. D. Brown, G. Pileio and M. H. Levitt, *Angew. Chem. Int. Ed.*, 2015, **54**, 3740–3743.
[34] Y. Zhang, X. Duan, P. C. Soon, V. Sychrovský, J. W. Canary and A. Jerschow, *ChemPhysChem*, 2016, **17**, 2967–2971.
[35] Z. Zhou, K. Claytor, W. S. Warren and T. Theis, *J. Magn. Reson.*, 2016, **263**, 108–115.
[36] S. J. Elliott, L. J. Brown, J.-N. Dumez and M. H. Levitt, *Phys. Chem. Chem. Phys.*, 2016, **18**, 17965–17972.
[37] S. J. Elliott, L. J. Brown, J.-N. Dumez and M. H. Levitt, *J. Magn. Reson.*, 2016, **272**, 87–90.
[38] J.-N. Dumez, B. Vuichoud, D. Mammoli, A. Bornet, A. C. Pinon, G. Stevanato, B. Meier, G. Bodenhausen, S. Jannin and M. H. Levitt, *J. Phys. Chem. Lett*, 2017, **8**, 3549–3555.
[39] P. Håkansson, *Phys. Chem. Chem. Phys.*, 2017, **19**, 10237–10254.
[40] S. Glöggler, S. J. Elliott, G. Stevanato, R. C. D. Brown and M. H. Levitt, *RSC Adv.*, 2017, **7**, 34574–34578.
[41] B. Kharkov, X. Duan, J. Canary and A. Jerschow, *J. Magn. Reson.*, 2017, **284**, 1–7.
[42] J. Bae, Z. Zhou, T. Theis, W. S. Warren and Q. Wang, *Sci. Adv.*, 2018, **4**, aar2978.
[43] S. J. Elliott, B. Meier, B. Vuichoud, G. Stevanato, L. J. Brown, J. Alonso-Valdesueiro, L. Emsley, S. Jannin and M. H. Levitt, *Phys. Chem. Chem. Phys.*, 2018, **20**, 9755–9759.
[44] S. Mamone and S. Glöggler, *Phys. Chem. Chem. Phys.*, 2018, **20**, 22463–22467.
[45] K. L. Ivanov, T. Kress, M. Baudin, D. Guarin, D. Abergel, G. Bodenhausen and D. Kurzbach, *J. Chem. Phys.*, 2018, **149**, 054202.
[46] S. J. Elliott, P. Kadeřávek, L. J. Brown, M. Sabba, S. Glöggler, D. J. O'Leary, R. C. D. Brown, F. Ferrage and M. H. Levitt, *Molecular Physics*, 2018, **0**, 1–7.
[47] J.-H. Ardenkjær-Larsen, B. Fridlund, A. Gram, G. Hansson, L. Hansson, M. H. Lerche, R. Servin, M. Thaning and K. Golman, *Proc. Natl. Acad. Sci. U.S.A.*, 2003, **100**, 10158–10163.
[48] A. Abragam, *Principles of Nuclear Magnetism*, Clarendon Press, Oxford, 1961.
[49] J. Cavanagh, W. J. Fairbrother, A. G. Palmer-III and N. Skelton, *Protein NMR Spectroscopy, 1st Ed.*, Academic Press, Massachusetts, 1995.
[50] A. Gryff-Keller and D. Kubica, *J. Phys. Chem. A*, 2012, **116**, 9632–9638.
[51] E. Chiavazza, E. Kubala, C. V. Gringeri, S. Düwel, M. Durst, R. F. Schulte and M. I. Menzel, *J. Magn. Reson.*, 2013, **227**, 35–38.
[52] D. Kubica, A. Wodyński, A. Kraska-Dziadecka and A. Gryff-Keller, *J. Phys. Chem. A*, 2014, **118**, 2995–3003.
[53] A. Gryff-Keller, S. Molchanov and A. Wodyński, *J. Phys. Chem. A*, 2014, **118**, 128–133.
[54] P. Bernatowicz, D. Kubica, M. Ociepa, A. Wodyński and A. Gryff-Keller, *J. Phys. Chem. A*, 2014, **118**, 4063–4070.
[55] G. Pileio, *J. Chem. Phys.*, 2011, **135**, 174502.
[56] J. Jeener, *Adv. Magn. Opt. Reson.*, 1982, **10**, 1–51.
[57] M. H. Levitt and L. Di Bari, *Phys. Rev. Lett.*, 1992, **69**, 3124–3127.
[58] T. O. Levante and R. R. Ernst, *Chem. Phys. Lett.*, 1995, **241**, 73–78.
[59] J. Kowalewski and L. Mäler, *Nuclear Spin Relaxation in Liquids: Theory, Experiments, and Applications*, CRC Press, Boca Raton, 2006.
[60] C. Bengs and M. H. Levitt, *Magn. Reson. Chem.*, 2017, **56**, 374–414.
[61] J. H. Van Vleck, *Phys. Rev.*, 1929, **33**, 467–506.

[62] H. Primas, *Rev. Mod. Phys.*, 1963, **35**, 710–711.
[63] A. W. E. Müller and A. R. M. Vásquez, *arXiv:quant-ph/9606011*, 1996.
[64] A. W. E. Müller and A. R. M. Vásquez, *arXiv:quant-ph/9606013*, 1996.
[65] K. Gottfried and T.-M. Yan, *Quantum Mechanics: Fundamentals*, Springer-Verlag New York, 2003.
[66] A. Jerschow, *Prog. Nucl. Magn. Reson. Spectrosc.*, 2005, **46**, 63–78.
[67] H. Hogben, M. Krzystyniak, G. Charnock, P. Hore and I. Kuprov, *J. Magn. Reson.*, 2011, **208**, 179–194.
[68] M. J. Frisch, G. W. Trucks, H. B. Schlegel, G. E. Scuseria, M. A. Robb, J. R. Cheeseman, G. Scalmani, V. Barone, B. Mennucci, G. A. Petersson, H. Nakatsuji, M. Caricato, X. Li, H. P. Hratchian, A. F. Izmaylov, J. Bloino, G. Zheng, J. L. Sonnenberg, M. Hada, M. Ehara, K. Toyota, R. Fukuda, J. Hasegawa, M. Ishida, T. Nakajima, Y. Honda, O. Kitao, H. Nakai, T. Vreven, J. A. Montgomery, J. E. Peralta, F. Ogliaro, M. Bearpark, J. J. Heyd, E. Brothers, K. N. Kudin, V. N. Staroverov, R. Kobayashi, J. Normand, K. Raghavachari, A. Rendell, J. C. Burant, S. S. Iyengar, J. Tomasi, M. Cossi, N. Rega, J. M. Millam, M. Klene, J. E. Knox, J. B. Cross, V. Bakken, C. Adamo, J. Jaramillo, R. Gomperts, R. E. Stratmann, O. Yazyev, A. J. Austin, R. Cammi, C. Pomelli, J. W. Ochterski, R. L. Martin, K. Morokuma, V. G. Zakrzewski, G. A. Voth, P. Salvador, J. J. Dannenberg, S. Dapprich, A. D. Daniels, Farkas, J. B. Foresman, J. V. Ortiz, J. Cioslowski and D. J. Fox, *Gaussian 09, Revision B.01*, Wallingford CT, 2009.
[69] W. C. Bailey, *J. Mol. Spectrosc.*, 1998, **190**, 318–323.
[70] M. C. D. Tayler and M. H. Levitt, *Phys. Chem. Chem. Phys.*, 2011, **13**, 9128–9130.
[71] C. Cohen-Tannoudji, B. Diu and F. Laloe, *Quantum Mechanics*, Wiley-VCH, 1991.